Modelling and Control of Cooperative Multi-Master/Multi-Slave Teleoperation Systems

MODELLING AND CONTROL OF COOPERATIVE MULTI-MASTER/MULTI-SLAVE TELEOPERATION SYSTEMS

BY

PEYMAN SETOODEH, B.Sc., M.Sc.

A THESIS

SUBMITTED TO THE DEPARTMENT OF ELECTRICAL & COMPUTER ENGINEERING

AND THE SCHOOL OF GRADUATE STUDIES

OF MCMASTER UNIVERSITY

IN PARTIAL FULFILMENT OF THE REQUIREMENTS

FOR THE DEGREE OF

MASTER OF APPLIED SCIENCE

Master of Applied Science (2006) McMaster University

(Electrical & Computer Engineering) Hamilton, Ontario, Canada

TITLE: Modelling and Control of Cooperative Multi-Master/Multi-Slave Teleoperation Systems

AUTHOR: Peyman Setoodeh

B.Sc., M.Sc., (Electrical Engineering)

Shiraz University, Shiraz, Iran

SUPERVISOR: Dr. Shahin Sirouspour

NUMBER OF PAGES: xi, 103

'Would you tell me, please, which way I ought to go from here?'

'That depends a good deal on where you want to get to,' said the Cat.

'I don't much care where—' said Alice.

'Then it doesn't matter which way you go,' said the Cat.

'—so long as I get SOMEWHERE,' Alice added as an explanation.

'Oh, you're sure to do that,' said the Cat, 'if you only walk long enough.'

— Lewis Carroll, Alice's Adventures in Wonderland.

Abstract

Cooperative teleoperation combines two traditional areas of robotics, i.e. teleoperation and collaborative manipulation. Cooperative telerobotic systems consist of multiple pairs of master/slave robotic manipulators operating in a shared environment. Due to dynamic interaction among slave manipulators as well as communication latency, control of such systems is particularly challenging and the application of standard teleoperation controller may result in instability.

In this thesis a multilateral control framework is proposed for cooperative teleoperation systems that allows for transmission of position and force information between all master and slave robots rather than merely between corresponding units. Two different control approaches are introduced that establish kinematic correspondence among masters and slaves. The operators are presented with a virtual intervening tool in order to collaboratively interact with the environment. Models of operators, master and slave robots, tool, and environment are incorporated in the design.

A multilateral adaptive nonlinear control architecture is proposed. Performance and stability of cooperative teleoperation systems are addressed under dynamic interactions between slave robots in the presence of model uncertainty. The robustness of the controller with respect to communication latency is also analyzed.

Simulation and experimental studies demonstrate that the proposed approach is highly effective in all phases of a teleoperation task, i.e. in free motion and in contact with both flexible and rigid environments.

The second approach involves finite-dimensional state-space models that incorporate the delay for free motion/soft contact as well as rigid contact modes of operation. Local dynamic linearization control laws are employed to linearize robotic manipulators' dynamics. Model-based discrete-time Linear Quadratic Gaussian (LQG) controllers are proposed that can deliver a stable transparent response for each phase of operation. The robustness of these controllers with respect to parameter uncertainty is examined via the Nyquist analysis. Simulation results demonstrate the effectiveness of the proposed approach.

Acknowledgements

I would like to sincerely thank and acknowledge my supervisor, Dr. Shahin Sirouspour for his continual support, technical and personal guidance, and trust. I am grateful to him for providing me many opportunities.

I am also grateful to Dr. Gary Bone and Dr. Shahram Shirani who served as the members of my supervisory committee for their valuable comments and feedback. I would also like to thank Dr. Tim Davidson for making a number of helpful suggestions.

Sincere thanks go to my friends and colleagues at Telerobotics, Haptics, and Computational Vision Lab, Ali Shahdi, Pouya Dehghani Tafti, Mahyar Fotoohi Ghiam, and Forough Farshidi for their kind helps and friendship.

I thank Cheryl Gies, Terry Greenlay, Cosmin Coroiu, and Helen Jachna who were always welcoming and helpful.

Finally, I would like to thank my family. Their endless support, encouragement, and love have always been a source of energy for me to pursue higher education.

Contents

List of Figures

Chapter 1

Introduction and Problem Statement

1.1 Motivation

The word *robot* was coined by the Czech playwright Karel Capek in his play Rossum's Universal Robots in 1920's. The word *robota* means forced labor or worker. According to the definition offered by Robot Institute of America in 1979, robot is a reprogrammable, multifunctional manipulator designed to move material, parts, tools, or specialized devices through various programmed motions for the performance of a variety of tasks [1].

In many applications a special task should be executed repeatedly with high accuracy in an environment that does not change drastically. Robots are good replacements for human operators in such applications. Employing robots in automatic assembly lines is a successful example. There are applications in which the task environment is inaccessible to human such as space operations and underwater exploration, or it is hazardous, i.e. toxic, chemical and nuclear material handling. Such tasks can be more effectively carried out by robots than human. In

micro and nano worlds, where human is unable to directly interact with the environment, employing of robots is indispensable. Also, there are applications in which the human's power should be scaled up. In most of these cases, the environment is unstructured and the tasks are not repetitive and sometimes are even unpredictable. Therefore, the design and control of fully autonomous robotic systems with the required degree of intelligence would be costly if not impossible [2]. Combining human intelligence with accuracy and manipulability of robots via *teleoperation* systems is an attractive solution to this problem.

The applications of teleoperation technology have been steadily growing over the past two decades in areas such as space operations, underwater exploration, and hazardous material handling. Such systems allow human operators to remotely interact with environments and to execute tasks via robots. They could also extend human handling capability at different scales both in macro and micro worlds. Recently teleoperation systems have been employed in medical sciences and entertainment industries successfully [2–5]. New applications are yet to be found.

People can carry out some tasks more effectively through collaboration rather than individual operation or by using their both hands instead of one hand. Similarly when compared with single-robot manipulation, cooperative manipulation has advantages such as increased dexterity, improved handling capability, increased loading capacity, and enhanced robustness due to redundancy. Cooperative teleoperation combines two traditional areas of robotics, i.e. teleoperation and collaborative manipulation.

Conventional single-master/single-slave (SMSS) teleoperation has been extensively studied before but cooperative teleoperation involves challenges that have not been considered in the design of conventional teleoperation systems. In cooperative teleoperation, multiple slave robots dynamically interact directly or through an intervening tool dynamics. Designs based on SMSS architectures fail to address the performance and stability requirements of cooperative teleoperation as they often neglect these interactions. The issues of performance and stability for such systems must be addressed under these constraints. Also the critical assumption of the passivity of the environment that the slave is in contact with, can be violated in cooperative environments. This implies that the use of controllers designed for conventional teleoperation, which ignore such interactions can potentially lead to instability in cooperative applications.

The goal of this research is to design, implement and evaluate control schemes for cooperative multi-master/multi-slave (MMMS) teleoperation systems. The controllers should achieve position and force tracking in free motion, and contact with flexible/rigid environments. Issues such as dynamic interactions between the slave robots and the task environment, unknown operator and environment dynamics as well as uncertainties in master and slave robots' models must be addressed in the controller design. The proposed research will also investigate the design of stable controllers in the presence of communication latency.

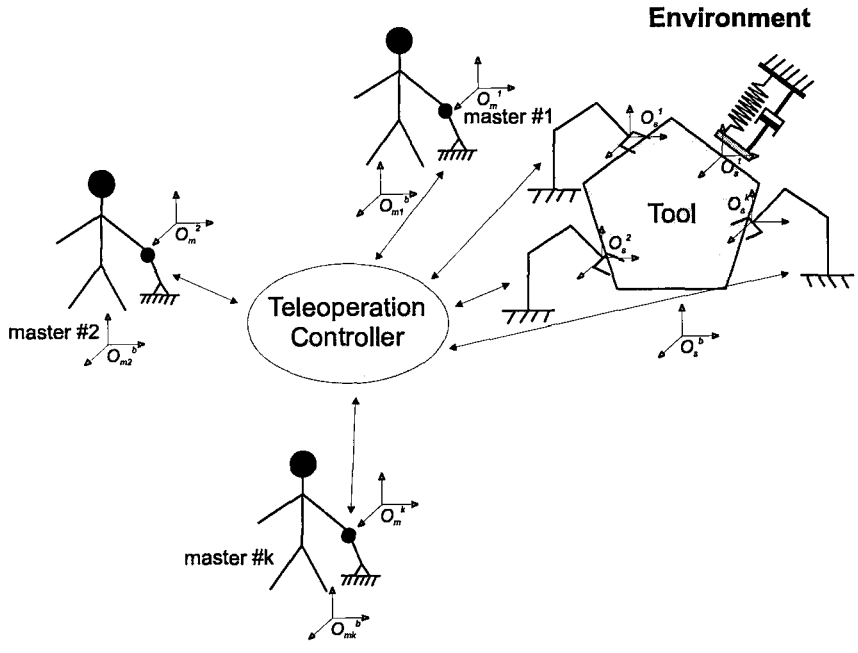

Figure 1.1: Schematic of a cooperative teleoperation system.

1.2 Problem Statement and Proposed Methodology

Cooperative teleoperation systems enable collaboration among several operators in performing a task via multiple pairs of master/slave robotic manipulators. Figure 1.1 displays a schematic cooperative teleoperation case in which m operators cooperatively work on environment through m slave manipulators and a tool. Proper performance criteria should be defined to address the cooperative issues. Controllers with centralized and decentralized structures will be proposed to achieve stability and satisfy the performance criteria. In the proposed architecture it is assumed that:

(i) Multiple operators control multiple slave manipulators in a coordinated manner to grasp a tool. Then the slave robots are rigidly in contact with the tool

and form a closed mechanical chain. The operators can move the tool in free motion, interact with a flexible environment, and bring the tool in contact with a rigid environment.

(ii) Position and force information is transmitted between all master and slave robots rather than merely between corresponding units.

(iii) In a centralized design, position and force data from all masters and slaves are sent to a central control unit and control commands based on the received information are sent to master and slave manipulators. The centralized controller could be located at either master or slave side.

(iv) In a decentalized scheme each master and slave will have a local controller that uses local information. Local controllers are responsible for robustness of the system against unknown operator and environment dynamics as well as model uncertainties. Coordination between masters and slaves is achieved by coordinating teleoperation controllers.

1.2.1 Advantages

The proposed architecture has several advantages:

(i) The extra communication links can be utilized to facilitate coordination among operators. For example, the controller can assist the operators in simultaneous grasping of an object through imposing virtual constraints on positions of the slaves and masters such that the slaves always keep the same distance from the object.

(ii) It is possible to impose a virtual intervening tool dynamics between the operators and the environment that they are working on. Therefore, the performance

of the operators will not be affected by a heavy tool.

(iii) In applications where communication delays are different throughout various channels, local information links can be utilized to reduce instability due to links with large delays. For instance, local exchange of force and position data between the masters and the slaves in teleoperation over long distances can facilitate task execution and reduce the risk of instability.

1.2.2 Challenges

There are several challenges that must be addressed in the design of a cooperative teleoperation system:

(i) Stability in the presence of dynamic interactions between slave manipulators and the task environment.

(ii) Stability in the presence of communication time delay.

(iii) Robustness against unknown operator and environment dynamics as well as master and slave model uncertainties.

1.3 Organization of the Thesis

The thesis is organized as follows. Telerobotic literature has been reviewed in Chapter 2, covering both conventional and cooperative teleoperation systems. An adaptive nonlinear controller is presented in Chapter 3 to address the presence of parametric uncertainty in the dynamics. Then Chapter 4 addresses the delay problem employing discrete-time Linear Quadratic Gaussian (LQG) controller. Chapter 5 contains simulation and experimental results in various scenarios. Finally, the

thesis is concluded in Chapter 6.

1.4 Related Publications

- P. Setoodeh, S. Sirouspour and A. Shahdi, "Discrete-time Multi-Model Control for Cooperative Teleoperation under Time Delay," *in Proc. IEEE International Conference on Robotics and Automation*, 2006 (to appear).
- S. Sirouspour and P. Setoodeh, "Multi-operator/multi-robot teleoperation: an adaptive nonlinear control approach," *in Proc. IEEE/RSJ International Conference on Intelligent Robots and Systems*, pp. 2506-2511, 2005.
- S. Sirouspour and P. Setoodeh, "Adaptive Nonlinear Teleoperation Control in Multi-master/Multi-slave Environments," *in Proc. IEEE Conference on Control Applications*, pp. 1263-1268, 2005.

Chapter 2

Literature Review

The following review contains representative examples of different approaches to teleoperation control.

2.1 Conventional Teleoperation

Five distinct elements constitute a conventional teleoperation system as shown in Figure 2.1. These are the human operator, master robot, controller and communication channel, slave robot, and the environment [4,5]. The human operator uses the master device to manipulate the environment through the slave robot. This operation is coordinated through the controller and communication block, which includes local and teleoperation controllers as well as the data communication channel. Based on the direction of information flow, the teleoperation may be unilateral or bilateral. In unilateral teleoperation, communication channel is utilized to send position and force data from master to slave and feedback visual information from slave to master. But in bilateral teleoperation, position and force data are also sent

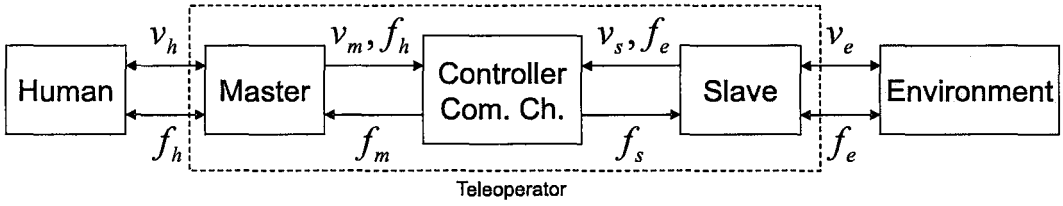

Figure 2.1: Model of a single-master/single-slave teleoperation system.

from slave to master in addition to the visual information. The communication channel introduces a round trip delay of $2T$ seconds in the control loop. When the operator sends a control command through the master manipulator, the slave receives the command after T seconds. Also, it takes another T seconds until the master receives information from the slave. Considering the response delay of the slave, it takes more than $2T$ seconds until the operator knows the result of his/her previous command.

The reported teleoperation control architectures in the literature, can be classified according to the type of information that is transferred between master and slave sides. These include position-position [6], position-force [7,8], force-force [9] and the four-channel bilateral teleoperation [10–12]. In the four-channel architecture, master and slave receive position/velocity and force data from the opposite side. Time delay in the communication channel can cause instability in teleoperation systems [13,14]. The wave-variables transformation and passivity-based controllers have been widely used in the literature to deal with the time delay problem. A comparative review of the proposed controllers for teleoperation systems in the presence of communication delay can be found in [15].

The goal of a teleoperation system is to provide the operators with the perception that they are directly executing the remote task. This measure of performance

is called transparency. Different transparency criteria have been defined in the literature such as master/slave position and force tracking or the equality of the environment mechanical impedance and the impedance felt by the operator [10]. Transparency and stability of the teleoperation system are two conflicting design requirements. The design of the teleoperation controllers involves a trade-off between robust stability and transparency [10]. Modelling and control techniques have been reported in the literature based on the linear circuit theory, linear robust control, feedback linearization, linear and nonlinear adaptive control, as well as the passivity-based control.

2.1.1 Methods Using Linear Circuit Theory

Using the well-known hybrid two-port models from circuit theory, Reference [7] proposed a bilateral impedance control architecture for teleoperation systems. In this framework, master and slave local controllers render approximations of the mechanical impedance that is seen at the opposite side. A thorough review of the application of the circuit theory to modelling and control of teleoperation systems has been presented in [12]. Also, the impedance model-based controllers were extended to four-channel bilateral teleoperation systems with admittance models. Following the approach of [16] a stability and performance robustness analysis based on the Llewellyn's absolute stability has been presented to account for the communication delay and operator as well as the environment dynamic uncertainties.

2.1.2 Methods Using Linear Robust Control Theory

An impedance shaping control scheme has been proposed in [17]. In this framework, a virtual environment is introduced that simulates the task iteratively to deal with different impedances and geometric scales. The robustness of the controller was analyzed using the structured singular value μ. In [9], H_∞-optimal control theory and model reduction techniques were used to control a force-force teleoperation system. A design procedure based on H_∞-optimal control and μ-synthesis was proposed in [8] that guarantees stability for a pre-specified upper bound on the communication time delay. In this approach, operator and environment impedances were assumed to be known. In [18] the H_∞ theory was employed to achieve a compromise between the optimization of performance criteria and robustness of bilateral teleoperation using first-order *Padé* approximation of the time delay. These approaches usually result in high dimensional matrices with high computational burden. The fixed-point implementation of H_∞ controllers has advantages from processing speed and memory space perspectives. References [19] and [20] studied the finite word length effects associated with this kind of implementation of H_∞ controllers for teleoperation systems.

2.1.3 Methods Using Feedback Linearization

Feedback linearization was utilized in first approaches to nonlinear control of teleoperation systems. In [21], nominal nonlinear models of master and slave robots were linearized. Then the boundedness of position and force tracking errors was proved via Lyapunov stability criterion by restricting the deviation of the model

from true system. In [22], a design procedure was presented to achieve robustness with respect to parameter uncertainty, external disturbance and measurement noise for the linearized dynamic models.

2.1.4 Methods Using Adaptive Control

Adaptive methods have been employed to deal with unknown operator and environment dynamics as well as uncertain master and slave models. Using linear time-invariant models for robots, an adaptive impedance reflecting control scheme based on the Slotine-Li algorithm [23] was proposed in [24]. The controller requires position, velocity and acceleration measurements. An adaptive controller for a single axis position-force teleoperation architecture was presented in [25].

While the first attempts used linear dynamic models of one degree-of-freedom (1 DOF) systems, recently adaptive algorithms have been applied to more complex nonlinear robot dynamics. In [26] a nonlinear adaptive control structure was proposed that employs full nonlinear dynamics of master and slave robots to guarantee stability and transparency. Models of human operator and flexible/rigid environment dynamics were integrated into the master and slave robot dynamics, respectively. Local adaptive controllers based on the Slotine-Li algorithm [23] were designed for master and slave to deal with unknown operator and environment dynamics as well as possible uncertainties in master and slave parameters within pre-specified bounds. Teleoperation controllers were designed to achieve position and force tracking both in free motion and contact with flexible and rigid

environments. Also, the stability in the presence of communication delay was analyzed. In [27] an adaptive approach that only estimates the master and slave dynamic parameters, was used to achieve similar closed-loop dynamics for master and slave manipulators. The algorithm does not estimate the human and environment parameters. In addition to local adaptive controllers of master and slave robots, a virtual master robot was introduced in [28]. This approach guarantees convergence of the position tracking error but the force tracking error depends on the acceleration of the designed virtual master.

2.1.5 Methods Using Passivity-Based Control

Since the feedback interconnection of passive subsystems is stable [29, 30], many authors have employed the passivity theory to design controllers for teleoperation systems with guaranteed stability. Master and slave robots are passive mechanical systems. Assuming passive operator and environment, the stability of the teleoperation system is guaranteed if the communication channel/controller remains passive.

The proposed controllers in [13] and [31] attempt to achieve a communication channel that resembles a lossless transmission line and therefore passive independent of the time delay. In [14], an adaptive tracking controller was proposed, which uses wave/scattering variables in a passivity-based framework. A survey on wave-variables and wave-based teleoperation could be found in [32]. In [33], Teleoperation system was considered as the interconnection of two port-controlled Hamiltonian systems through a transmission line with constant time delay and the adaptation of port-Hamiltonian systems with dissipation to the transmission line

was studied. In [34] online automatic tuning of the wave impedance parameter was proposed to improve performance under varying task configurations, i.e. free motion and contact with environment.

Although the passivity-based controllers guarantee the stability of the teleoperation system, they are often conservative and degrade the performance. Also, they do not guarantee position and force tracking in general. A modified version of these controllers was proposed in [35], which kinematically locks the master and slave robots by a coordination controller. The proposed controller achieves bounded force tracking error. It should be noted that the methods proposed in the above references are energy-based and deal with constant time delays in the communication channel. Recently a time-domain passivity-based controller, has been proposed for teleoperation without delay under a wide variety of environments and operating speeds [36]. In [37] practical limitations of wave-based controllers in non-ideal situations, which cause loss of passivity were investigated and a method for restoring the passivity was proposed.

2.1.6 Teleoperation over Digital Communication Channels

The growing use of the Internet as the communication medium in teleoperation systems, has introduced new challenges for researchers. It introduces variable time delays and causes loss of passivity. Approaches such as introducing energy-monitoring methods [38], inserting time-varying gain in the transmission path [39], and using fictitious energy storage [40] have been proposed in the literature. The discretization of a passive system via sample and hold, could yield a non-passive

system [41]. References [42] and [43] have proposed methods for preserving passivity of the interconnection of continuous and discrete time systems. Recently teleoperation control techniques that are directly applicable in the presence of digital communication channels have attracted attention of researchers.

In [44] and [45] the sampled-data nature of the controller has been taken into account. Also, methods for energy dissipation have been proposed to preserve passivity in the presence of variable time delay, packet loss, and quantization errors introduced by position encoders. In [46] and [47] a buffering and interpolation-based method has been proposed to preserve passivity in a teleoperation system that uses packet-switched networks for communication.

In [48], the concept of telemonitoring force feedback for teleoperation under short time delays is introduced. Other techniques such as predictive displays rely on accurate models of the task environment to provide the operator with a realistic delay-free simulated response of the remote manipulator and environment [49,50]. Predictive control methods such as the Smith Predictor have also been developed for teleoperation [15, 51]. In [51], the wave-based teleoperation controller is combined with a Smith Predictor, a Kalman Filter, and an energy regulator to improve the performance.

Teleoperation problem has been formulated in discrete-time domain in [52]. This approach allows for a finite dimension state-space model that explicitly includes the time delay. Discrete-time Linear Quadratic Gaussian (LQG) controllers that deliver a transparent stable response in the presence of constant delay have been proposed in this method. Unknown variable delays are estimated and can be made constant through synchronization and buffering [53]. The LQG controller

yields delay-free position and force tracking between master and slave both in free motion and in contact, although in transitions the tracking is achieved after d sampling periods.

2.2 Cooperative Teleoperation

Despite the extensive amount of research in teleoperation and coordinated control of robots, MMMS teleoperation has received little attention in the past. This includes the work in [54–56], which proposes the use of heuristic methods such as predictive graphic displays to address the time delay in the communication channels in cooperative telerobotic environments. Development of a software for Internet-based distributed multiple-telerobot system that enables operators to use remote robots in order to perform cooperative tasks has been reported in [57].

An event-based control approach using Petri-Net modelling and analysis tools was proposed in [58] for MMMS systems in free motion. The goal of the controller is to telecoordinate slave robots via the Internet according to a pre-specified quantitative coordination index. Telecoordination is achieved by making robots event-transparent and event-synchronous. In cases that the next command does not arrive before the next event reference increment, slaves will wait and the system behaves similar to a move and wait system.

A semi-autonomous control architecture was proposed in [59] for single-master /multi-slave (SMMS) teleoperation systems. In this framework, a local controller provides a stable grasp at the slave side and locks the slave robots and the grasped object together as an abstract single slave. Then this abstract slave is controlled

from the master side through a conventional bilateral teleoperation controller. Wave variables were utilized to guarantee stability of the closed loop system in the presence of communication delay. The proposed controller was evaluated through simulation in [60].

It should be noted that all of the above approaches either ignore the dynamic interactions between slave robots or just achieve coordination in free motion. A multi-lateral control architecture for MMMS teleoperation has been presented in [61]. The proposed framework incorporates flow of position and force information between all master and slave robots. Within this architecture, cooperative performance measures are defined to enhance coordination among the operators and the robots for achieving task objectives. A μ-synthesis-based methodology for cooperative teleoperation control was introduced. This approach guarantees robust stability of cooperative teleoperation in the presence of dynamic interaction between slave robots as well as unknown passive operators and environment dynamics. It also improves task coordination by minimizing relevant performance objectives. Effectiveness of the proposed approach was demonstrated by simulation and experimental studies on a two master/two-slave one-axis system both in free motion and in contact with flexible or rigid environments.

Chapter 3

Adaptive Nonlinear Control for Cooperative Teleoperation

3.1 Introduction

This chapter proposes an adaptive nonlinear controller for cooperative teleoperation systems to accommodate nonlinearities and parametric uncertainties. The control laws are inspired by those given in [26] for conventional single-master/singleslave (SMSS) teleoperation. The major contribution is extending such control approach to cooperative teleoperation applications where multiple masters and slaves are involved.

The proposed multilateral teleoperation controller establishes position-position kinematic correspondence between the masters and slaves. It also synthesizes an adjustable intervening tool impedance between the operators and the environment. The stability of the closed-loop system in free motion, in contact with flexible environments, and in contact with rigid environments is demonstrated via

Lyapunov analysis. The novelty of the proposed cooperative controller is due to: (i) explicitly addressing the issues of performance and stability in the presence of dynamic interaction between the slaves as well as in the presence of parametric uncertainty in the models of operators and the environment. This is in contrast with the few reported work in cooperative teleoperation which either do not consider such dynamic interactions or only study the problem of free motion coordination. (ii) its data communication architecture which allows for all possible information routs.

3.2 Nonlinear System Dynamics in Cooperative Teleoperation

In the cooperative teleoperation system of Figure 1.1, the slaves/tool interaction can be as simple as the slaves grasping a rigid tool or as complex as the slaves handling a multi-body system. Only rigid linear tool dynamics are examined here but the formulation can be extended to other cases such as multi-body rigid and deformable tool dynamics [62].

The i'th master's rigid body dynamics are governed by the following second-order nonlinear differential equation:

$$\ddot{x}_m^i + C_m^i(x_m^i, \dot{x}_m^i)\dot{x}_m^i + G_m^i(x_m^i) = f_m^i + f_h^i \tag{3.1}$$

where $x_m^i \in R^6$ is the generalized position of a frame attached to the i'th master's handle w.r.t. its base frame. f_m^i is the equivalent control action at the handle and

f_h^i is the i'th operator's force exerted on the master both expressed in the base frame. It should be noted that the $f_m^i = {J_m^i}^T \tau_m^i$ where J_m^i is a Jacobian matrix relating the joint velocities to work-space velocities and τ_m^i is the vector of actuators force/torque expressed in the joint-space. For reasons that will become obvious later, these dynamics are transformed to a new coordinate frame representing the position of a virtual tool through the mapping $\Phi^i(.)$.

$$\bar{M}_m^i(\Phi^i(x_m^i))\ddot{\Phi}^i(x_m^i) + \bar{C}_m^i(\Phi^i(x_m^i), \dot{\Phi}^i(x_m^i))\dot{\Phi}^i(x_m^i) + \bar{G}_m^i(\Phi^i(x_m^i)) = \bar{f}_m^i + \bar{f}_h^i \quad (3.2)$$

where $\bar{f}_m^i$ and $\bar{f}_h^i$ are the transformed control action and hand force, respectively. In (3.2), $\bar{M}_m^i$ is the mass matrix, $\bar{C}_m^i$ models coriolis and centripetal effects, and $\bar{G}_m^i$ represents the effect of gravity. These matrices have some special properties that will be used throughout this chapter for stability analysis [63].

The operators' arm dynamics are approximated by a second-order linear time-invariant differential equation.

$$M_h^i\ddot{\Phi}^i(x_h^i) + B_h^i\dot{\Phi}^i(x_h^i) + K_h^i\Phi^i(x_h^i) = \bar{f}_h^{*i} - \bar{f}_h^i \quad (3.3)$$

where $M_h^i > 0$, $B_h^i > 0$, and $K_h^i > 0$ are mass, damping and stiffness matrices of the operator's arm, respectively. $\Phi^i(x_h^i)$ is the generalized hand position transformed to the virtual tool frame. $\bar{f}_h^{*i}$ is the operator's intentional force and is assumed to be bounded, i.e. $|\bar{f}_h^{*ij}| < f_{max}^{ij}$ where f_{max}^i is an upper bound on the intentional hand force of the i'th operator.

Remark 3.1: The dynamics of the arm are in general nonlinear, time-dependent,

and posture-dependent. However, previous researchers have successfully employed linear models in their work [26, 64]. The arm parameters are assumed constant but otherwise unknown.

When the operator holds the master handle, i.e. $x_m^i = x_h^i$, the dynamics of master and operator in (3.2) and (3.3) can be integrated as follows

$$M_{mh}^i \ddot{\Phi}^i(x_m^i) + C_{mh}^i(\Phi^i(x_m^i), \dot{\Phi}^i(x_m^i))\dot{\Phi}^i(x_m^i) + G_{mh}^i(x_m^i) \\ = Y_{mh}^i \left(\ddot{\Phi}^i(x_m^i), \dot{\Phi}^i(x_m^i), \dot{\Phi}^i(x_m^i), \Phi^i(x_m^i)\right) \theta_{mh}^i = \bar{f}_m^i + \bar{f}_h^{*i} \quad (3.4)$$

with $M_{mh}^i = \bar{M}_m^i + M_h^i$, $C_{mh}^i = \bar{C}_m^i + B_h^i$, and $G_{mh}^i = \bar{G}_m^i + K_h^i$. In (3.4), $Y_{mh}^i \theta_{mh}^i$ is the linear-in-parameter representation of the dynamics with θ_{mh}^i being the vector of unknown parameters of the operator and possibly the master arm [63].

The dynamics of the slave robots are similar to those of the master robots. For the i'th slave one may write

$$M_s^i(x_s^i)\ddot{x}_s^i + C_s^i(x_s^i, \dot{x}_s^i)\dot{x}_s^i + G_s^i(x_s^i) = f_s^i - f_t^i \quad (3.5)$$

where x_s^i is the generalized position of a frame attached to the contact point of the i'th slave and tool represented in the slaves' base frame. f_s^i is the equivalent control action in the end-effector frame, and f_t^i is the reaction force from the tool both expressed in the base frame. It is assumed that the slave manipulators and the tool form a closed kinematic chain which imposes the following constraint on the positions of the slaves and the tool.

$$x_t = \Psi^1(x_s^1) = \Psi^2(x_s^2) = \cdots = \Psi^m(x_s^m) \quad (3.6)$$

with x_t being the generalized position of a frame attached to the tool at its potential contact point with the environment with respect to the base frame. Ψ's are appropriate nonlinear coordinate transformations. The tool and end-effector velocities are related through the tool Jacobian matrices defined below:

$$\dot{x}_t = \frac{\partial \Psi^1}{\partial x_s^1}\dot{x}_s^1 = \frac{\partial \Psi^2}{\partial x_s^2}\dot{x}_s^2 = \cdots = \frac{\partial \Psi^m}{\partial x_s^m}\dot{x}_s^m \tag{3.7}$$

The dynamics of the tool can be written as

$$M_t\ddot{x}_t + B_t\dot{x}_t + K_t x_t = \sum_{i=1}^{m} J_t^{iT} f_t^i - f_e \tag{3.8}$$

where $M_t > 0$, $B_t > 0$, and $K_t > 0$ are constant but otherwise unknown mass, damping and stiffness of the tool, respectively. $J_t^i = \left(\frac{\partial \Psi^i}{\partial x_s^i}\right)^{-1}$ and f_e is a generalized force exerted on the environment by the tool at its contact point.

Dynamics of the slave robots and the tool can be combined using (3.5)-(3.8) to obtain

$$M_{st}(x_t)\ddot{x}_t + C_{st}(x_t, \dot{x}_t)\dot{x}_t + G_{st}(x_t) = \sum_{i=1}^{m} J_t^{iT} f_s^i - f_e \tag{3.9}$$

and

$$\begin{aligned} M_{st} &= M_t + \textstyle\sum_{i=1}^{m} J_t^{iT} M_s^i J_t \\ C_{st} &= B_t + \textstyle\sum_{i=1}^{m} (J_t^{iT} M_s^i \dot{J}_t^i + J_i^T C_s^i J_t^i) \\ G_{st} &= K_t + \textstyle\sum_{i=1}^{m} J_t^{iT} G_s^i \end{aligned} \tag{3.10}$$

Environment reaction force f_e is modelled assuming that the tool-environment

contacts are rigid along some *a priori known directions* and are flexible along the rest. To simplify the analysis and without loss of generality, it is further assumed the slaves' base frame has been selected such that rigid and flexible coordinates are decoupled in generalized tool position vector x_t in (3.9).

Remark 3.2: It should pointed out that depending on the geometry and configuration of the environment, the flexible and rigid directions may or may not be orthogonal. The slaves' base frame and the nonlinear transformations in (3.6) can be chosen accordingly to satisfy the decoupling requirement.

Note that x_t in (3.9) can be written as

$$x_t = \Delta_r x_e^r + (I - \Delta_r)\, x_t \tag{3.11}$$

and Δ_r is a 6×6 diagonal matrix such that

$$\Delta_r^{ii} = \begin{cases} \delta_r^i & \text{contact is rigid} \\ 0 & \text{contact is flexible} \end{cases} \tag{3.12}$$

and

$$\delta_r^i = \begin{cases} 1 & \text{contact in i'th direction} \\ 0 & \text{free motion} \end{cases} \tag{3.13}$$

x_e^r in (3.11) is a vector of constant contact positions along the rigid directions.

Therefore,

$$\Delta_r \dot{x}_t = 0$$
$$\Delta_r \ddot{x}_t = 0 \tag{3.14}$$

The environment reaction force f_e can be written in terms of its flexible and rigid components as follows

$$f_e = \Delta_r f_e + \Delta_f \left(M_e \ddot{x}_t + B_e \dot{x}_t + K_e x_t \right) \tag{3.15}$$

where $\Delta_r f_e = f_r$ is a vector of environment reaction forces along the rigid coordinates. $M_e \geq 0$, $B_e \geq 0$, $K_e \geq 0$ are constant matrices that model the dynamics of the flexible part of the environment. It should be pointed out that the rows and columns associated with rigid coordinates are zero and therefore these matrices are only positive-semi definite. Δ_f for flexible contact is defined similar to Δ_r for rigid contact, i.e.

$$\Delta_f^{ii} = \begin{cases} \delta_f^i & \text{contact is flexible} \\ 0 & \text{contact is rigid} \end{cases} \tag{3.16}$$

and,

$$\delta_f^i = \begin{cases} 1 & \text{contact in i'th direction} \\ 0 & \text{free motion} \end{cases} \tag{3.17}$$

Using (3.9), (3.11), and (3.15), the combined dynamics of the slaves, tool, and the

environment may be written as

$$M_{ste}\ddot{x}_t + C_{ste}(x_t, \dot{x}_t)\dot{x}_t + G_{ste} = Y_{ste}\left(\ddot{x}_t, \dot{x}_t, \dot{x}_t, x_t\right)\theta_{ste} = \sum_{i=1}^{m} J_t^{iT} f_s^i - \Delta_r f_e \quad (3.18)$$

with

$$\begin{aligned} M_{ste} &= M_{st} + \Delta_f M_e \\ C_{ste} &= B_{st} + \Delta_f B_e \\ G_{ste} &= G_{st} + \Delta_f K_e \end{aligned} \quad (3.19)$$

The vector θ_{ste} includes unknown parameters of the flexible environment and possibly the slave robots and the tool. This completes the derivation of the dynamics of the cooperative teleoperation system.

3.3 Adaptive Nonlinear Control for Masters and Slaves

The first step in deriving the cooperative teleoperation controllers is to design adaptive nonlinear control laws for master and slave robots. These controllers are similar to those in [26] with two exceptions: First, there are multiple slave manipulators and a tool here which form a kinematic chain and therefore their dynamics are coupled. In [26] only one slave is considered. Second, Reference [26] divides the contact space into two rigid and flexible subspaces. The modelling here is slightly different as it permits several flexible and rigid contact coordinates. In other words, all flexible or rigid contacts do not necessarily occur simultaneously. Figure 3.1 depicts the structure of the controller.

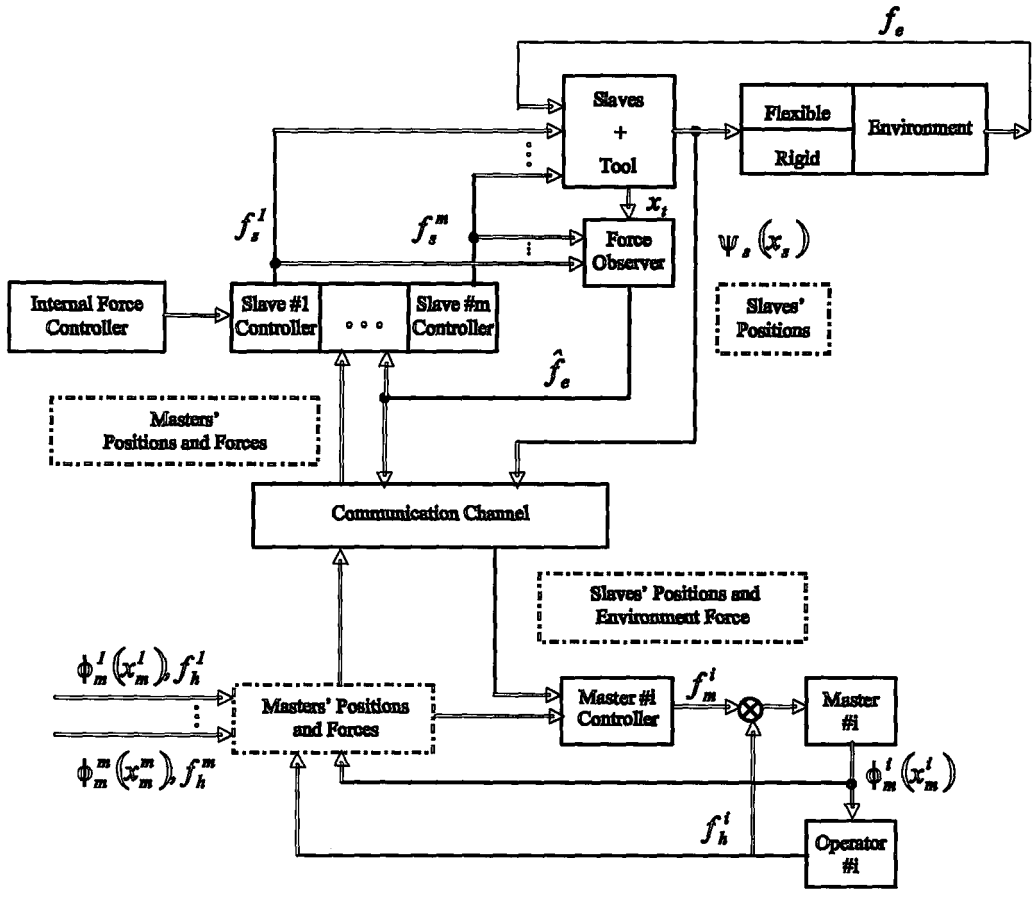

Figure 3.1: The structure of the adaptive nonlinear controller for cooperative teleoperation.

3.3.1 Control Laws

The control laws for the slave robots are given by

$$F_s = J_t^{\dagger} u_s + F_s^{int}$$
$$F_s = \begin{bmatrix} f_s^1 & \dots & f_s^m \end{bmatrix}^T \tag{3.20}$$

where

$$u_s = Y_{ste}\left(\dot{v}_t^r, v_t^r, \dot{x}_t, x_t\right)\hat{\theta}_{ste} + K_s\rho_t + A_s^{-1}\Delta_r\left(C^{-1}\dot{v}_t^d + v_t^d\right)$$
$$v_t^r = v_t^d - A_s\tilde{f}_e$$
$$\rho_t = v_t^r - v_t \tag{3.21}$$

and $K_s, C, A_s > 0$ are diagonal matrices. v_t^d is tool velocity command. $\tilde{f}_e$ is a filtered environment reaction force that will be introduced in the next section. The slaves' control action $F_s \in R^{mn}$ while $x_t \in R^n$. F_s^{int} is an internal force component that does not affect the motion of the tool, i.e. $J_t F_s^{int} = 0$. To resolve the redundancy in slaves' actuation, one may choose

$$J_t^{\dagger} = Q^{-1}J_t^T\left[J_tQ^{-1}J_t^T\right]^{-1} \tag{3.22}$$
$$F_s^{int} = 0 \tag{3.23}$$

where $J_t = \begin{bmatrix} J_t^{1T} & \cdots & J_t^{mT} \end{bmatrix}$. This will minimize the scaled norm of control action vector $\|Q^{\frac{1}{2}}F_s\|$ [65,66]. Alternatively, F_{int}^s can be any vector in the null space of J_t^T, i.e.

$$F_s^{int} = \left(I - J_t^{\dagger}J_t\right)f \tag{3.24}$$

and $f \in R^{mn}$ is arbitrary. One possible form for F_s^{int} in the case that m is an even number is given by

$$F_s^{int} = \begin{bmatrix} J_t^{1^{-1}} & -J_t^{2^{-1}} & J_t^{3^{-1}} & \cdots & -J_t^{m-1} \end{bmatrix}^T f_{int}^d \tag{3.25}$$

The internal force F_s^{int} can help maintain the contact between the slave manipulators and the tool if the end-effectors are not equipped with grippers.

The slave/environment parameter adaptation is driven by

$$\dot{\hat{\theta}}_{ste} = \Gamma_s Y_{ste}^T \left(\dot{v}_t^r, v_t^r, \dot{x}_t, x_t\right) \rho_t = \Gamma_s y_\theta \tag{3.26}$$

where Γ_s is a diagonal matrix with elements

$$\gamma^{ii} = \begin{cases} 0 & \hat{\theta}_s^i \leq \theta_s^{min^i}, y_\theta^i \leq 0 \\ 0 & \hat{\theta}_s^i \geq \theta_s^{max^i}, y_\theta^i \geq 0 \\ \gamma_s^i & \text{otherwise} \end{cases} \tag{3.27}$$

$\gamma^{i'}$s are positive and θ_s^{min} and θ_s^{max} are known lower and upper bounds on the parameters.

The Control command for the i'th master is computed using

$$\begin{aligned} f_m^i &= Y_{mh}^i \left(\dot{v}_m^{ri}, v_m^{ri}, \dot{\Phi}^i(x_m^i), \Phi^i(x_m^i)\right) \hat{\theta}_{mh}^i + K_m^i \rho_m^i + f_{max}^i \text{sgn}(\rho_m^i) \\ v_m^{ri} &= v_m^{di} + K_p^{-1} A_m^i \tilde{f}_h^i \\ \rho_m^i &= v_m^{ri} - \dot{\Phi}^k(x_m^i) \end{aligned} \tag{3.28}$$

$K_m^i, \Lambda, K_p, A_m > 0$ are diagonal. $\tilde{f}_h^i$ is a filtered hand force. The i'th master/operator parameter adaptations are given by

$$\dot{\hat{\theta}}_{mh}^i = \Gamma_m^i Y_{mh}^T \left(\dot{v}_m^{ri}, v_m^{ri}, \dot{\Phi}^i(x_m^i), \Phi^i(x_m^i)\right) \rho_m^i = \Gamma_m^i z_\theta^i \tag{3.29}$$

where Γ_m^i is a diagonal matrix with elements

$$\gamma^{jj} = \begin{cases} 0 & \hat{\theta}_{mh}^{ij} \leq \theta_{mh}^{min^{ij}}, z_\theta^{ij} \leq 0 \\ 0 & \hat{\theta}_{mh}^{ij} \geq \theta_{mh}^{max^{ij}}, z_\theta^{ij} \geq 0 \\ \gamma_{mh}^{ij} & \text{otherwise} \end{cases} \tag{3.30}$$

γ^{ij}'s are positive and $\theta_{mh}^{min^i}$ and $\theta_{mh}^{max^i}$ are known lower and upper bounds on the master/arm parameters.

3.3.2 Stability Analysis

The following closed-loop error dynamics are obtained for the slaves/tool/evironment subsystem by substituting the slaves' control law in (3.21) into (3.18) and after some manipulation

$$\left[M_{ste} + \Delta_r C^{-1} A_s^{-1}\right] \dot{\rho}_t + \left[C_{ste} + \Delta_r A_s^{-1} + K_s\right] \rho_t - Y_{ste} \tilde{\theta}_{ste} = 0 \tag{3.31}$$

with $\tilde{\theta}_{ste} = \theta_{ste} - \hat{\theta}_{ste}$. The following is a Lyapunov function for the error dynamics in (3.31)

$$V_s = \frac{1}{2} \rho_t^T \left[M_{ste} + \Delta_r C^{-1} A_s^{-1}\right] \rho_t + \frac{1}{2} \tilde{\theta}_{ste}^T {\Gamma_s}^{-1} \tilde{\theta}_{ste} \tag{3.32}$$

Differentiating (3.32) with respect to time and recalling that $\dot{\tilde{\theta}}_{ste} = -\dot{\hat{\theta}}_{ste}$, yields

$$\dot{V}_s = \rho_t^T \left[M_{ste} + \Delta_r C^{-1} A_s^{-1}\right] \dot{\rho}_t - \dot{\hat{\theta}}_{ste}^T {\Gamma_s}^{-1} \tilde{\theta}_{ste} \tag{3.33}$$

Solving (3.31) for $\dot{\rho}_t$ and substituting in (3.33) gives

$$\dot{V}_s = -\rho_t^T \left[C_{ste} + \Delta_r A_s^{-1} + K_s\right] \rho_t + \rho_t^T Y_{ste} \tilde{\theta}_{ste} - \dot{\hat{\theta}}_{ste}^T {\Gamma_s}^{-1} \tilde{\theta}_{ste} \tag{3.34}$$

Using (3.26), it is not difficult to show that

$$\dot{V}_s \leq -{\rho_t}^T \left[\Delta_r A_s^{-1} + K_s\right] \rho_t \tag{3.35}$$

Similarly, the i'th master/operator closed-loop dynamics are governed by

$$\begin{aligned} M_{mh}^i(\Phi^i(x_m^i))\dot{\rho}_m^i + C_{mh}^i(\Phi^i(x_m^i), \dot{\Phi}^i(x_m^i))\rho_m^i + K_m^i \rho_m^i \\ + \tilde{f}_h^{*i} + f_{max}^i \text{sgn}(\rho_m^i) - Y_{mh}^i \tilde{\theta}_m^i = 0 \end{aligned} \tag{3.36}$$

with $\tilde{\theta}_m^i = \theta_m^i - \hat{\theta}_m^i$. A Lyapunov function for these error dynamics is given by

$$V_m^i = \frac{1}{2} {\rho_m^i}^T M_{mh}^i \rho_m^i + \frac{1}{2} {\tilde{\theta_m^i}}^T {\Gamma_m^i}^{-1} \tilde{\theta}_m^i \tag{3.37}$$

Again, differentiating (3.37) with respect to time and recalling that $\dot{\tilde{\theta}}_m^i = -\dot{\hat{\theta}}_m^i$, yields

$$\dot{V}_m^i = {\rho_m^i}^T M_{mh}^i \dot{\rho}_m^i - {\dot{\hat{\theta}}_m^i}^T {\Gamma_m^i}^{-1} \tilde{\theta}_m^i \tag{3.38}$$

Solving (3.36) for $\dot{\rho}_m^i$ and substituting in (3.38) gives

$$\begin{aligned} \dot{V}_m^i = -{\rho_m^i}^T \left[C_{mh}^i + K_m^i\right] \rho_m^i - {\rho_m^i}^T \left[f_h^{*i} + f_{max}^i \text{sgn}(\rho_m^i)\right] \\ + {\rho_m^i}^T Y_{mh}^i \tilde{\theta}_m^i - {\dot{\hat{\theta}}_m^i}^T {\Gamma_m^i}^{-1} \tilde{\theta}_m^i \end{aligned} \tag{3.39}$$

Using (3.29), it can be demonstrated that

$$\dot{V}_m^i \leq -{\rho_m^i}^T K_m^i \rho_m^i \tag{3.40}$$

The results in (3.32)-(3.40) yield

$$\begin{aligned} \rho_m^i &= v_m^{di} - \dot{\Phi}(x_m^i) + A_m^i \tilde{f}_h^i \in L_2 \bigcap L_\infty, \quad i = 1, \cdots, m \\ \rho_t &= v_t^d - v_t - A_s \tilde{f}_e \in L_2 \bigcap L_\infty \end{aligned} \tag{3.41}$$

Remark 3.3: The stability results have been derived assuming constant Δ_r and Δ_f. Further investigation is required for the incorporation of contact transition phases into the controller design and stability analysis.

Remark 3.4: The switching terms in the masters' control law (3.28) eliminate the error due to unknown bounded external force f_h^{*i}. However, high frequency switching activities are undesirable because they can excite system's high frequency modes and cause instability. They can also negatively impact the life of the actuators. In practice, this can be resolved by replacing the sgn() with a smooth function. Alternatively, f_h^* may be included in θ_m and estimated on-line. Such approach is effective if the rate of change in f_h^* is slow with respect to the time constant of parameter adaption. The latter approach is adopted in this work.

3.4 Teleoperation Coordinating Controllers

Local adaptive nonlinear controllers in (3.20) and (3.28) guarantee the stability of ρ_m^i and ρ_t. The operation of masters and slaves are coordinated through the design

of desired velocity commands v_m^{di} in (3.28) and v_t^d in (3.21) as follows:

$$v_m^{di} = \frac{K_p^{-1}}{2m}\sum_{k=1}^{m}\dot{\tilde{\Psi}}^k(x_s^k) + \frac{K_p^{-1}}{2m}\Lambda\sum_{k=1}^{m}\left[\tilde{\Psi}^k(x_s^k) - K_p\Phi^i(x_m^i)\right] + \frac{1}{2m-2}\sum_{k=1,\neq i}^{m}\dot{\tilde{\Phi}}^k(x_m^k) + \frac{\Lambda}{2m-2}\sum_{k=1,\neq i}^{m}\left[\tilde{\Phi}^k(x_m^k) - \Phi^i(x_m^i)\right] + K_p^{-1}\sum_{k=1,\neq i}^{m}A_m^k\tilde{f}_h^k - K_p^{-1}A_s\tilde{f}_e \quad (3.42)$$

$$v_t^d = \frac{K_p}{m}\sum_{k=1}^{m}\dot{\tilde{\Phi}}^k(x_m^k) + K_p\Lambda\left[\frac{1}{m}\sum_{k=1}^{m}\tilde{\Phi}^k(x_m^k) - K_p^{-1}x_t\right] + \sum_{k=1}^{m}A_m^k\tilde{f}_h^k \quad (3.43)$$

In the above formulation

$$\begin{aligned}\dot{\tilde{\Phi}}^k(x_m^k) + C\tilde{\Phi}^k(x_m^k) &= C\Phi^k(x_m^k)\\ \dot{\tilde{\Psi}}^k(x_s^k) + C\tilde{\Psi}^k(x_s^k) &= C\Psi^k(x_s^k)\\ \dot{\tilde{f}}_h^k + C\tilde{f}_h^k &= C\bar{f}_h^k\\ \dot{\tilde{f}}_e + C\tilde{f}_e &= Cf_e\end{aligned} \quad (3.44)$$

Using (3.20),(3.28),(3.42), and (3.43), it can be shown

$$\rho_m^i - \rho_m^j = \frac{1}{2m-2}[\dot{\tilde{\Phi}}^j(x_m^j) - \dot{\tilde{\Phi}}^i(x_m^i) + \Lambda\left(\tilde{\Phi}^j(x_m^j) - \tilde{\Phi}(x_m^i)\right)] + \dot{\Phi}^j(x_m^j) - \dot{\Phi}^i(x_m^i) + \Lambda\left(\Phi^j(x_m^j) - \Phi^i(x_m^i)\right) \quad (3.45)$$

Equation (3.45) can be written as

$$\rho_m^i - \rho_m^j = \frac{1}{2m-2}\tilde{\Omega} + \Omega \tag{3.46}$$

with

$$\Omega = \dot{\Phi}^j(x_m^j) - \dot{\Phi}^i(x_m^i) + \Lambda\left(\Phi^j(x_m^j) - \Phi^i(x_m^i)\right) \tag{3.47}$$

and

$$\dot{\tilde{\Omega}} + C\tilde{\Omega} = C\Omega \tag{3.48}$$

Using (3.46), (3.48) and the fact that $\rho_m^i - \rho_m^j \in L_2 \bigcap L_\infty$,

$$\Omega \in L_2 \bigcap L_\infty \tag{3.49}$$

which yields the following results

$$\Phi^j(x_m^j) - \Phi^i(x_m^i) \in L_2 \bigcap L_\infty \tag{3.50}$$

$$\dot{\Phi}^j(x_m^j) - \dot{\Phi}^i(x_m^i) \in L_2 \bigcap L_\infty \tag{3.51}$$

and therefore the position tracking error between the i'th and j'th master devices is stable. Furthermore,

$$\rho_t - \frac{K_p}{m}\sum_{k=1}^{m}\rho_m^k = \frac{1}{2m}\sum_{k=1}^{m}\left[K_p\dot{\tilde{\Phi}}^k(x_m^k) - \dot{\tilde{\Psi}}^k(x_s^k)\right] + \\ + \frac{1}{2m}\Lambda\sum_{k=1}^{m}\left[K_p\tilde{\Phi}^k(x_m^k) - \tilde{\Psi}^k(x_s^k)\right] + \\ \left[\frac{K_p}{m}\sum_{k=1}^{m}\dot{\Phi}^k(x_m^k) - v_t\right] + \Lambda\left[\frac{K_p}{m}\sum_{k=1}^{m}\Phi^k(x_m^k) - x_t\right] \quad (3.52)$$

Again given that $\rho_t - \frac{K_p}{m}\Sigma_{k=1}^{m}\rho_m^k \in L_2 \bigcap L_\infty$ and following similar steps to (3.46)-(3.48), it can be shown that

$$\frac{K_p}{m}\sum_{k=1}^{m}\Phi^k(x_m^k) - x_t \in L_2 \bigcap L_\infty \quad (3.53)$$

$$\frac{K_p}{m}\sum_{k=1}^{m}\dot{\Phi}^k(x_m^k) - v_t \in L_2 \bigcap L_\infty \quad (3.54)$$

Therefore, the stability of tracking errors between scaled masters' and slaves' positions is guaranteed. Next, the force tracking behavior of the proposed cooperative teleoperation controller is studied.

$$\rho_t + \frac{K_p}{m}\sum_{k=1}^{m}\rho_m^k = \frac{K_p}{m}\sum_{k=1}^{m}\left[\dot{\tilde{\Phi}}^k(x_m^k)v_m^k - \dot{\Phi}^k(x_m^k)\right] + \left[\frac{1}{m}\sum_{k=1}^{m}\dot{\tilde{\Psi}}^k(x_s^k) - v_t\right] + \frac{K_p}{m}\Lambda\sum_{k=1}^{m}\left[\tilde{\Phi}^k(x_m^k) - \Phi^k(x_m^k)\right] + \Lambda\left[\frac{1}{m}\sum_{k=1}^{m}\tilde{\Psi}^k(x_s^k) - x_t\right] + \frac{1}{2m}\sum_{k=1}^{m}\left[K_p\dot{\tilde{\Phi}}^k(x_m^k) - \dot{\tilde{\Psi}}^k(x_s^k)\right] + \frac{1}{2m}\Lambda\sum_{k=1}^{m}\left[K_p\tilde{\Phi}^k(x_m^k) - \tilde{\Psi}^k(x_s^k)\right] + 2\sum_{k=1}^{m}A_m^k\tilde{f}_h^k - 2A_s\tilde{f}_e \quad (3.55)$$

It should be noted that

$$\begin{aligned}
\tilde{\Phi}^k(x_m^k) - \Phi^k(x_m^k) &= -C^{-1}\dot{\tilde{\Phi}}^k(x_m^k)\\
\tilde{\Psi}^k(x_s^k) - x_t &= -C^{-1}\dot{\tilde{\Psi}}^k(x_s^k)\\
\dot{\tilde{\Phi}}^k(x_m^k) - \dot{\Phi}^k(x_m^k) &= -C^{-1}\ddot{\tilde{\Phi}}^k(x_m^k)\\
\dot{\tilde{\Psi}}^k(x_s^k) - v_t &= -C^{-1}\ddot{\tilde{\Psi}}^k(x_s^k)
\end{aligned} \quad (3.56)$$

and also from (3.52),

$$\begin{aligned}
&\tfrac{1}{2m}\textstyle\sum_{k=1}^{m}\left[K_p\dot{\tilde{\Phi}}^k(x_m^k) - \dot{\tilde{\Psi}}^k(x_s^k)\right] \in L_2 \bigcap L_\infty\\
&\tfrac{1}{2m}\Lambda\textstyle\sum_{k=1}^{m}\left[K_p\tilde{\Phi}^k(x_m^k) - \tilde{\Psi}^k(x_s^k)\right] \in L_2 \bigcap L_\infty
\end{aligned} \quad (3.57)$$

Using (3.55)-(3.57) results in

$$2\sum_{k=1}^{m} A_m \tilde{f}_h^k - 2A_s\tilde{f}_e - \frac{K_p C^{-1}}{m}\sum_{k=1}^{m}\ddot{\tilde{\Phi}}^k(x_m^k) - \frac{C^{-1}}{m}\sum_{k=1}^{m}\ddot{\tilde{\Psi}}^k(x_s^k) - \frac{K_p C^{-1}\Lambda}{m}\sum_{k=1}^{m}\dot{\tilde{\Phi}}^k(x_m^k) - \frac{C^{-1}\Lambda}{m}\sum_{k=1}^{m}\dot{\tilde{\Psi}}^k(x_s^k) \in L_2\bigcap L_\infty \quad (3.58)$$

Note that

$$A_s\tilde{f}_e = A_s\Delta_r\tilde{f}_e + A_s\Delta_f\tilde{f}_e \quad (3.59)$$

and from (3.20) and (3.43)

$$A_s\Delta_r\tilde{f}_e = \Delta_r v_t^d - \Delta_r\rho_t = \frac{K_p}{m}\Delta_r\sum_{k=1}^{m}\dot{\tilde{\Phi}}^k(x_m) + \frac{K_p\Lambda}{m}\Delta_r\sum_{k=1}^{m}\tilde{\Phi}^k(x_m^k) - \Lambda x_t + \Delta_r\sum_{k=1}^{m}A_m\tilde{f}_h^k - \Delta_r\rho_t \quad (3.60)$$

and using (3.15)

$$A_s\Delta_f\tilde{f}_e = A_s\left(M_e\ddot{\tilde{x}}_t + B_e\dot{\tilde{x}}_t + K_e\tilde{x}_t\right) \quad (3.61)$$

Also

$$\tilde{f}_h^k = \tilde{f}_h^{*k} - M_h^k\ddot{\tilde{\Phi}}^k(x_m^k) - B_h^k\dot{\tilde{\Phi}}^k(x_m^k) - K_h^k\tilde{\Phi}^k(x_m^k) \quad (3.62)$$

with

$$\dot{\tilde{f}}_h^{*k} + C\tilde{f}_h^{*k} = C\bar{f}_h^{*k} \tag{3.63}$$

Following conclusions are drawn by substituting (3.59)-(3.62) into (3.58),

$$\tilde{\Phi}^k(x_m^k), \dot{\tilde{\Phi}}^k(x_m^k) \in L_\infty \tag{3.64}$$

$$\tilde{\Psi}^k(x_s^k), \dot{\tilde{\Psi}}^k(x_s^k) \in L_\infty \tag{3.65}$$

$$\Phi^k(x_m^k), \dot{\Phi}^k(x_m^k) \in L_\infty \tag{3.66}$$

$$\Psi^k(x_s^k), \dot{\Psi}^k(x_s^k) \in L_\infty \tag{3.67}$$

This completes the proof of stability for the closed-loop system. Using a rigorous analysis similar to that in [26], it is possible to show that ρ_m^i's and ρ_t converge to zero. The convergence of position tracking errors to zero can then be concluded.

Now by letting $A_m = K_f A$, $A_s = A$, and assuming that the frequency of operation is below the bandwidth of the first-order filter $C/2\pi$, (3.61) can be approximated by

$$\Sigma_{k=1}^m \bar{f}_h^k - K_f^{-1} f_e \approx K_f^{-1} K_p A^{-1} C^{-1} \left[\ddot{\Phi}(x_m) + \Lambda \dot{\Phi}(x_m)\right] \tag{3.68}$$

This can be interpreted as a virtual intervening tool dynamics with a mass of $K_f^{-1}K_pA^{-1}C^{-1}$ and damping of $K_f^{-1}K_pA^{-1}C^{-1}\Lambda$ acting between the scaled environment force K_f^{-1} and the operators' net force $\Sigma_{k=1}^m \bar{f}_h^k$. The mass and stiffness of virtual tool are adjustable by the control parameters A, C, K_p, K_f, and Λ. Figure 3.2 illustrates the concept of the virtual intervening tool between the operators and the

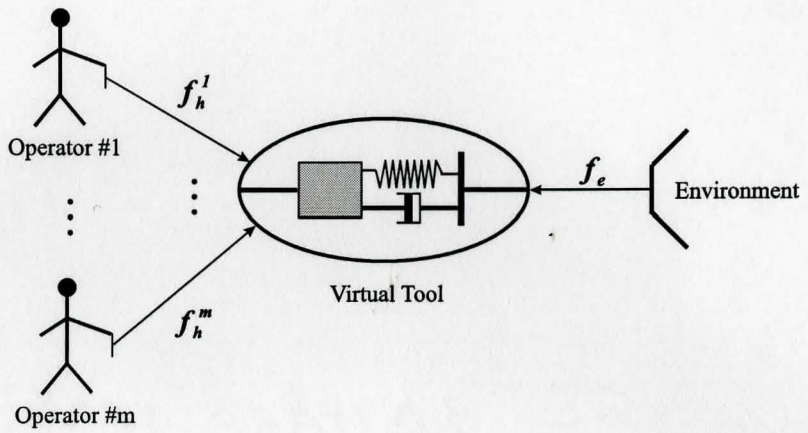

Figure 3.2: Virtual intervening tool between operators and environment.

environment.

Remark 3.5: The controller implementation requires the knowledge of Δ_r. In practice this can be determined from force and position measurements as the forces are nonzero while the contact velocities are zero along the rigid contact directions.

Remark 3.6: Time delay in the communication channels has not been considered in the cooperative teleoperation controller. Inclusion of such delays are critical for teleoperation over long distances.

3.5 The Effect of Communication Delay

In this section, the stability of the proposed controller in the presence of time delay in communication channels is analyzed. It is assumed that the time delay in the local communication links between the masters as well as between the slaves is negligible compared to the one-way time delay, T, between the master and slave sites. This time delay is assumed to be constant. Due to the presence of the delay,

(3.42) and (3.43) are modified as follows

$$v_m^{di} = \frac{1}{2m-2}\sum_{k=1,\neq i}^{m}\dot{\tilde{\Phi}}^k(x_m^k) + \frac{\Lambda}{2m-2}\sum_{k=1,\neq i}^{m}\left[\tilde{\Phi}^k(x_m^k) - \Phi^i(x_m^i)\right] + \frac{K_p^{-1}}{2m}\Lambda\sum_{k=1}^{m}\left[e^{-sT}\tilde{\Psi}^k(x_s^k) - K_p\Phi^i(x_m^i)\right] + e^{-sT}\frac{K_p^{-1}}{2m}\sum_{k=1}^{m}\dot{\tilde{\Psi}}^k(x_s^k) + K_p^{-1}\sum_{k=1,\neq i}^{m}A_m^k\tilde{f}_h^k - e^{-sT}K_p^{-1}A_s\tilde{f}_e \quad (3.69)$$

$$v_t^d = e^{-sT}\frac{K_p}{m}\sum_{k=1}^{m}\dot{\tilde{\Phi}}^k(x_m^k) + K_p\Lambda\left[\frac{1}{m}e^{-sT}\sum_{k=1}^{m}\tilde{\Phi}^k(x_m^k) - K_p^{-1}x_t\right] + e^{-sT}\sum_{k=1}^{m}A_m^k\tilde{f}_h^k \quad (3.70)$$

By substituting (3.69) and (3.70) into (3.41) and considering $\tilde{f}_h^k = \tilde{f}_h^{\star k} - Z_h^k\dot{\tilde{\Phi}}^k(x_m^k)$, $Z_h^k = Z_k$, $A_m^k = A_m$, and $\tilde{f}_e = Z_e\tilde{v}_t$, it can be shown that

$$H_{1s}(s)\tilde{P}_s = H_{2s}(s)e^{-sT}\tilde{P}_m - \tilde{\rho}_s \quad (3.71)$$

$$H_{1m}(s)\tilde{P}_m = H_{2m}(s)e^{-sT}\tilde{P}_s - \tilde{\rho}_m \quad (3.72)$$

where $\tilde{P}_s = \tilde{x}_t$, $\tilde{P}_m = \sum\tilde{\Phi}^k(x_m^k)$, and

$$\tilde{\rho}_s = \rho_t - e^{-sT}A_m\textstyle\sum_{k=1}^{m}\tilde{f}_h^{\star k}$$
$$\tilde{\rho}_m = \textstyle\sum_{k=1}^{m}\rho_m^k - mK_p^{-1}A_m\sum_{k=1}^{m}\tilde{f}_h^{\star k} \quad (3.73)$$

$$
\begin{aligned}
H_{2s}(s) &= \tfrac{K_p}{m}\left(sI+\Lambda\right) - A_m Z_h \\
H_{1s}(s) &= \left(s+\Lambda\right)\left(C^{-1}s+I\right) + A_s Z_e s \\
H_{2m}(s) &= \tfrac{mK_p^{-1}}{2}\left[sI+\Lambda-2A_s Z_e s\right] \\
H_{1m}(s) &= \left(sI+\Lambda\right)\left(sC^{-1}+\tfrac{1}{2}I\right) + mK_p^{-1}A_m Z_h s
\end{aligned} \tag{3.74}
$$

Using (3.71) and (3.72),

$$\tilde{P}_s = H_{1s}^{-1}(s)H_{2s}(s)H_{1m}^{-1}(s)H_{2m}(s)e^{-2sT}\tilde{P}_s - \rho_s^* \tag{3.75}$$

$$\tilde{P}_m = H_{1m}^{-1}(s)H_{2m}(s)H_{1s}^{-1}(s)H_{2s}(s)e^{-2sT}(\tilde{P}_m) - \rho_m^* \tag{3.76}$$

$$\rho_s^* = H_{1s}^{-1}\tilde{\rho}_s + H_{1s}^{-1}(s)H_{2s}(s)H_{1m}^{-1}(s)e^{-sT}\tilde{\rho}_m \tag{3.77}$$

$$\rho_m^* = H_{1m}^{-1}\tilde{\rho}_s + H_{1m}^{-1}(s)H_{2m}(s)H_{1s}^{-1}(s)e^{-sT}\tilde{\rho}_s \tag{3.78}$$

Since ρ_s and ρ_m are bounded according to (3.41), the system remains stable for any time delay if:

$$\left\|H_{1s}^{-1}(j\omega)H_{2s}(j\omega)H_{1m}^{-1}(j\omega)H_{2m}(j\omega)\right\|_\infty < 1 \tag{3.79}$$

$$\left\|H_{1m}^{-1}(j\omega)H_{2m}(j\omega)H_{1s}^{-1}(j\omega)H_{2s}(j\omega)\right\|_\infty < 1 \tag{3.80}$$

The controller parameters can be obtained through formulating a min-max optimization problem characterized by (3.79) and (3.80). The maximization and minimization are performed over ω and controller parameters, respectively. Additional constraints can be imposed on the mass and damping of the virtual tool in (3.68) to achieve a desired performance. The equivalent mass and damper of the virtual

tool in (3.68) contribute to transparency error. In order to reduce the transparency error, large A and C are required. However, it was shown in [26] that $\|AC\|$ should be limited for maintaining stability. Therefore, the choice of A and C specifies the tradeoff between stability and transparency.

Chapter 4

Discrete-Time LQG Control for Cooperative Teleoperation

4.1 Introduction

This chapter introduces a discrete-time Linear Quadratic Gaussian (LQG) controller for cooperative teleoperation systems. The treatment of the problem in the discrete-time domain is motivated by the fact that time delay can be modelled by finite dimension states in the discrete time. The proposed control framework utilizes a fully connected communication network between all master and slave units. Therefore each master and slave robot can receive position and force information from all master and slave units. In our approach, the latency is assumed to be *a priori* known constant. Unknown variable delays can be estimated and made constant through synchronization and buffering [53].

The environment dynamics can vary widely in a teleoperation task and hence

introduce significant uncertainty into the system model. To mitigate this problem, multiple controllers along with proper switching rules are employed instead of a single controller for the entire range of the operation. Such an adaptive approach is less conservative and can yield superior performance over single-mode controllers [67]. In the proposed controller, delayed measurement and control signals are first incorporated into the system's state-space model. The discrete-time LQG algorithm is then used to synthesize model-based output-feedback controllers that are optimized for transparency. The performance indices used include non-delayed position tracking, force tracking, and virtual tool impedance shaping.

4.2 Linearized System Dynamics in Cooperative Teleoperation

This chapter addresses the problem of cooperative teleoperation depicted in Figure 1.1, where the slaves rigidly hold a tool in order to manipulate the environment. In Figure 1.1, the tool frame O_s^t expresses the position of the tool with respect to the slaves' base frame O_s^b. The closed kinematic chain formed by the slave robots and the tool imposes the following constraint on the motion of the slaves:

$$V_s = J_t^T v_t \tag{4.1}$$

where v_t is the generalized velocity of the tool frame w.r.t. the base frame and $V_s = \begin{bmatrix} v_s^{1^T} & \cdots & v_s^{m^T} \end{bmatrix}^T$ is a vector of slaves' end-effector velocities w.r.t. the same frame. $J_t = \begin{bmatrix} J_s^1 & \cdots & J_s^m \end{bmatrix}$ and $J_s^{k^T}$ is a Jacobian matrix relating the k'th slave's

end-effector velocity to the tool velocity. The slave/tool interaction forces in the slaves' end-effector frames produce a net force acting on the tool frame, i.e.

$$f_e = \begin{bmatrix} J_s^1 \cdots & J_s^m \end{bmatrix} F_s = J_t F_s \tag{4.2}$$

with $F_s = \begin{bmatrix} f_s^{1^T} & \cdots & f_s^{m^T} \end{bmatrix}^T$, f_s^i is the force that the i'th slave robot exerts on the tool.

In general the dynamics of robotic manipulators are nonlinear and position-dependent. However, such dynamics can be rendered linear through the application of local dynamic linearization control laws [63]. The dynamics of the i'th slave manipulators after application of the nonlinear controllers are

$$J_s^{i^{-1}} z_s^i J_s^{i^{-T}} v_s^i = J_s^{i^{-1}} f_{cs}^i - f_s^i \tag{4.3}$$

where f_{cs}^i is the i'th slave equivalent control vector acting at O_s^t expressed in O_s^b and z_s^i is the linearized impedance observed from O_s^t. Using (4.1) and (4.3), the i'th slave dynamics in the tool frame can be written as

$$m_s^i \ddot{x}_t + b_s^i \dot{x}_t + k_s^i x_t = f_{cs}^i - J_s^i f_s^i \tag{4.4}$$

with m_s, b_s, and k_s being transformed dynamic parameters. Considering linear second order dynamics for the tool and compliant environments in the tool frame, the slaves, tool and the environment dyanmics can be combined to obtain:

$$(m_{st} + \sigma_f m_e)\ddot{x}_t + (b_{st} + \sigma_f b_e)\dot{x}_t + (k_{st} + \sigma_f k_e)x_t = \sum_{i=1}^{m} f_{cs}^i - \sigma_f f_e^* \tag{4.5}$$

where m_{st}, b_{st}, and k_{st} are the combined mass, damping, and stiffness of tool and slave robots, respectively. m_e, b_e, and k_e are environment dynamic parameters, and f_e^* is the exogenous environment force. Also, $\sigma_f = 1$ when the tool is in contact with a flexible environment and otherwise is zero.

During a rigid contact, the slaves' acceleration and velocity are zero and the environment force is equal to the slaves' control actions. Therefore, contact with a rigid environment can be modelled as

$$m_{st}(1-\sigma_r)\ddot{x}_t + b_{st}(1-\sigma_r)\dot{x}_t + k_{st}(1-\sigma_r)x_t = \sum_{i=1}^{m} f_{cs}^i - \sigma_r f_e \tag{4.6}$$

where f_e was defined in (4.2), and $\sigma_r = 1$ when the tool is in contact with a rigid environment and otherwise is zero.

The nonlinear dynamics of the master manipulators can be linearized similarly. When the i'th operator holds the corresponding master handle, i.e. $x_m^i = x_h^i$, the linearized dynamics of master and operator can be integrated as follows:

$$m_{mh}^i \ddot{x}_m^i + b_{mh}^i \dot{x}_m^i + k_{mh}^i x_m^i = f_{cm}^i + f_h^{*i} \tag{4.7}$$

where m_{mh}^i, b_{mh}^i, and k_{mh}^i are the combined mass, damping, and stiffness, respectively, x_m^i is the i'th master/hand position, f_{cm}^i is the control signal, and f_h^{*i} is the operator's intentional force modelled as an exogenous input to the system. The vectors are all related to corresponding master virtual tool frame O_m^i and are expressed in the i'th master base frame O_{mi}^b.

Throughout the rest of this chapter, it is assumed that the linearized dynamics are decoupled in different axes of motion. It should be noted that during contact,

a coupling among the axes may exist due to the presence of a tangential friction force that is proportional to the normal force. However if the contact along the normal axis is stable, the normal force and hence the tangential friction force are bounded and can be treated as disturbance to the motion in the tangential axis. Such disturbances can be handled by the controller that will be introduced in this paper. Considering the above assumptions, a single-axis problem is considered here though the proposed control approach can be extended to the full six-axis case [68–71].

4.3 LQG Teleoperation Control

The performance of conventional single-master/single-slave telerobotic systems is measured by their transparency. In an ideally transparent telerobotic system, the operator should feel that he/she is directly interacting with the environment. This notion of transparency, can be described in terms of position and force tracking between the master and slave robots [5,11].

$$f_h = \alpha_f f_e \tag{4.8}$$

$$x_m = \alpha_p x_s \tag{4.9}$$

where α_f and α_p scale the force and position tracking between the master and slave. Acceleration measurement or equivalently force measurement, and the exact knowledge of the master and slave dynamics are required for achieving the ideal transparency.

Unfortunately in a perfectly transparent system, modelling errors can cause

instability because of the complete cancellation of the master and slave dynamics (e.g. a negative mass can be produced) [11]. A modified version of transparency defines a virtual intervening tool between the operator and the environment [5,11].

$$f_h = m_{vt}\ddot{x}_{vt} + b_{vt}\dot{x}_{vt} + k_{vt}x_{vt} + \alpha_f f_e \tag{4.10}$$

$$x_m = \alpha_p x_s \tag{4.11}$$

where m_{vt}, b_{vt}, and k_{vt} are mass, damping, and stiffness of the virtual tool. While in a transparent system according to (4.8)-(4.9), the operator interacts with the task environment through a rigid tool without dynamics, the modified transparency measures introduce an intervening virtual tool with desired mass-spring-damper dynamics. The tool parameters should be selected such that sufficient stability margins are gained without compromising the operator's perception of the environment through a dominant tool dynamics.

It should be noted that in rigid contact, the modified transparency requirements in (4.10)-(4.11) reduce to original force and position tracking measures in (4.8)-(4.9), if $k_{vt} = 0$.

These transparency criteria can be extended to the cooperative teleoperation case as

$$\sum_{i=1}^{m} f_h^i - \alpha_f f_e = m_{vt}\ddot{x}_{vt} + b_{vt}\dot{x}_{vt} + k_{vt}x_{vt} \tag{4.12}$$

$$\frac{1}{m}\sum_{i=1}^{m} x_m^i = \alpha_p x_t \tag{4.13}$$

$$x_m^i = x_m^j \tag{4.14}$$

where m_{vt}, b_{vt}, and k_{vt} are the desired virtual tool parameters (Figure 3.2). The

system dynamics in (4.7)-(4.6) and the performance indices in (4.12)-(4.14) are all expressed in the continuous-time domain. In practice, the system outputs are sampled and the control actions are applied at a fixed rate. The control signal is constant between the sampling instants. The transformation of the dynamics and the performance measures into the discrete-time domain allows for direct discrete control synthesis. The application of a zero-order-hold continuous to discrete transformation [72] results in the following dynamics for the i'th operator/master subsystem:

$$X^i_{mh}[n+1] = A^i_{mh}X^i_{mh}[n] + B^i_{mh}f^i_{cm}[n] + G^i_{mh}w^i_{mh}[n] \tag{4.15}$$

where $X^i_{mh}[n] = \begin{bmatrix} x^i_m[n] & v^i_m[n] \end{bmatrix}^T$ is the state vector. The disturbance signal is $w^i_{mh}[n] = \begin{bmatrix} f^{*i}_h[n] & \tilde{f}^i_{cm}[n] \end{bmatrix}^T$ where $\tilde{f}^i_{cm}[n]$ is the disturbance in the control signal $f^i_{cm}[n]$.

Similarly, the slaves/tool/environment dynamics can be written as

$$X^{mode}_{ste}[n+1] = A^{mode}_{ste}X^{mode}_{ste}[n] + B^{mode}_{ste}f_{cs}[n] + G^{mode}_{ste}w_{ste}[n] \tag{4.16}$$

where the superscript *mode* shows the mode of operation; free motion, contact with a flexible environment, and contact with a rigid environment. For free motion/contact with flexible environment $X_{ste}[n] = \begin{bmatrix} x_t[n] & v_t[n] \end{bmatrix}^T$ while for contact with rigid environment $X_{ste}[n] = \begin{bmatrix} x_t[n] & f_e[n] \end{bmatrix}^T$. The control signal is $f_{cs}[n] = \sum_{i=1}^m f^i_{cs}$ and the disturbance vector is $w_{ste}[k] = \begin{bmatrix} f^*_e[n] & \tilde{f}_{cs}[n] \end{bmatrix}^T$. The state transition matrices are function of the operation *mode*. Note that in rigid contact the

slave robot's state vector includes the environment force $f_e[n]$. In practice, the controller implementation introduces one sample delay and hence $f_e[n] = f_{cs}[n-1]$. The derivation of elements of A^i_{mh}, B^i_{mh}, G^i_{mh}, A^{mode}_{ste}, B^{mode}_{ste}, and G^{mode}_{ste} is straightforward and will not be presented here. The desired virtual tool dynamics in (4.12) can also be converted to the discrete-time domain

$$X_{vt}[n+1] = A_{vt}X_{vt}[n] + B_{vt}u_{vt}[n] \tag{4.17}$$

where $X_{vt}[n] = \begin{bmatrix} x_{vt}[n] & v_{vt}[n] \end{bmatrix}^T$ and $u_{vt}[n] = \begin{bmatrix} f^1_h[n] & \cdots & f^m_h[n] & f_e[n] \end{bmatrix}^T$.

Teleoperation controllers are often distributed between the master and slave sites due to the distribution of system dynamics. In this thesis it is assumed that the time delay in the local communication links between the masters as well as between the slaves is negligible compared to the one-way time delay, between the master and slave sites. According to this assumption, the master controllers receive non-delayed position/force information from other masters and delayed position/force information from the slaves. On the other hand, the slave controllers use non-delayed data from other slaves and delayed information from the masters. Nevertheless, the LQG control is a centralized design approach which utilizes all measurements in generating the control signals. Therefore, controller must be placed either at the master end or at the slave end. Throughout this chapter, it is assumed that the controller resides at the operators' end as displayed in Figure 4.1. Similarly the controller could be placed at the slaves' end.

The structural change in the slave/enviroment dynamics due to rigid contact and parameter variations due to flexible contact can be handled with a multi-model control approach [73,74]. Model-based controllers are designed for different

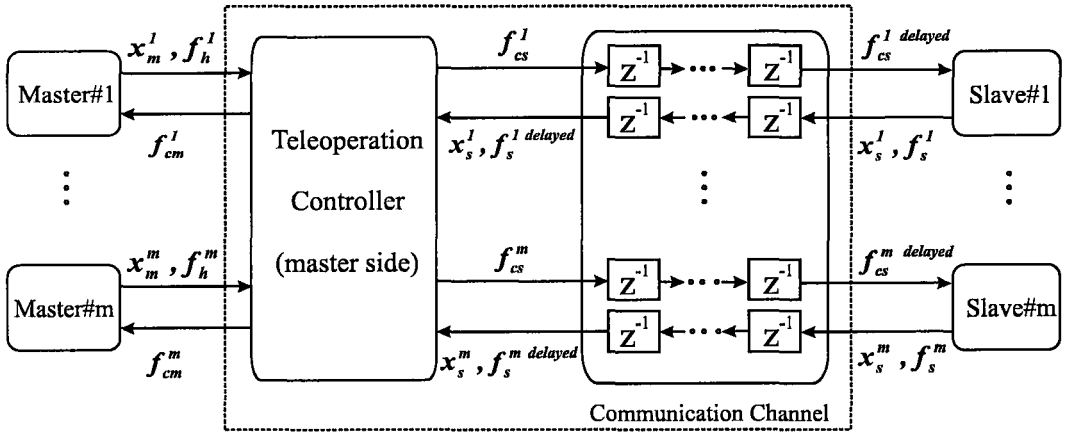

Figure 4.1: Cooperative teleoperation controller resides at the master side.

phases of the operation. Switching between these controllers occurs according to the estimated contact state. In this strategy, a controller is designed for free motion, another controller handles flexible contacts while a third controller is employed for interacting with rigid environments. Alternatively, it is possible to design a single controller that can function for both free motion and flexible contact, although such an approach would be more conservative. The schematic of the LQG cooperative teleoperation controller is displayed in Figure 4.2.

4.3.1 Free Motion/Soft Contact

The states of the system for the cases of free motion/soft contact are defined as follows

$$X[n] = \begin{bmatrix} X_m^1[n]^T & \cdots & X_m^m[n]^T & X_{ste}[n]^T & X_{vt}[n]^T \end{bmatrix}^T \tag{4.18}$$

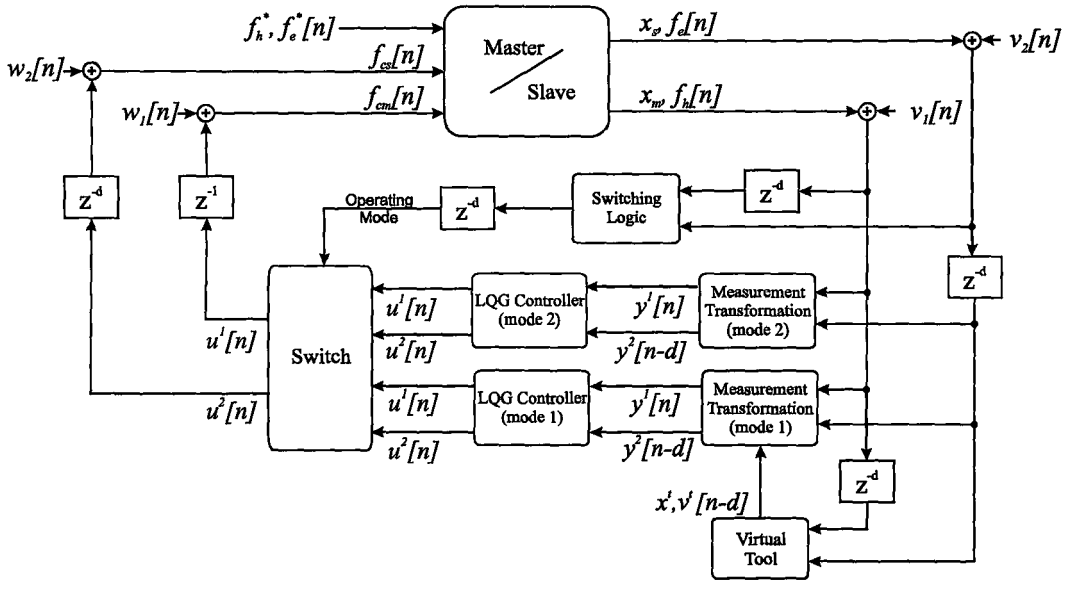

Figure 4.2: The LQG teleoperation control system with $x_m[n] = [x_m^1[n] \cdots x_m^m[n]]^T$, $f_h[n] = [f_h^1[n] \cdots f_h^m[n]]^T$, and $f_{cm}[n] = [f_{cm}^1[n] \cdots f_{cm}^m[n]]^T$.

where $X_{vt}[n]$ has been introduced in (4.17), and $X_m^i[n]$ and $X_s[n]$ are defined as follows in order to coordinate the behavior of the masters, slaves and virtual tool [75].

$$X_m^i[n] = \sum_{k=1,\neq i}^{m} [h_{m_k}^i (X_{mh}^i[n] - X_{mh}^k[n])] + h_s^i (X_{mh}^i[n] - \alpha_p X_{ste}[n]) + h_{vtm}^i (X_{mh}^i[n] - X_{vt}[n]) \quad (4.19)$$

$$X_s[n] = \sum_{k=1}^{m} [h_{s_k} (X_{ste}[n] - \frac{1}{\alpha_p} X_{mh}^k[n])] + h_{vts} (X_{ste}[n] - \frac{1}{\alpha_p} X_{vt}[n]) \quad (4.20)$$

$h_{m_k}^i$, h_s^i, h_{vtm}^i, h_{s_k}, and h_{vts} are weighting factors and α_p is position scale factor between masters and slaves. The above choice of states facilitates the application of the LQG method by explicitly including the tracking errors of interest into the

state vector. The states evolution is governed by

$$X[n+1] = AX[n] + Bu[n] + Gw[n] \tag{4.21}$$

$$u[n] = \begin{bmatrix} f_{cm}[n]^T & f_{cs}[n] \end{bmatrix}^T \tag{4.22}$$

$$w[n] = \begin{bmatrix} f_h^*[n]^T & f_e^*[n] & \tilde{f}_{cm}^T & \tilde{f}_{cs}[n] \end{bmatrix}^T \tag{4.23}$$

where

$$f_{cm}[n] = \begin{bmatrix} f_{cm}^1[n] & \cdots & f_{cm}^m[n] \end{bmatrix}^T \tag{4.24}$$

$$f_h^*[n] = \begin{bmatrix} f_h^{*1}[n] & \cdots & f_h^{*m}[n] \end{bmatrix}^T \tag{4.25}$$

$$\tilde{f}_{cm}[n] = \begin{bmatrix} \tilde{f}_{cm}^1[n] & \cdots & \tilde{f}_{cm}^m[n] \end{bmatrix}^T \tag{4.26}$$

It is straightforward to obtain the system matrices, A, B, G from A_{mh}^i, B_{mh}^i, C_{mh}^i, D_{mh}^i, G_{mh}^i, H_{mh}^i, A_{ste}, B_{ste}, C_{ste}, D_{ste}, G_{ste}, H_{ste}, A_{vt}, and B_{vt}, and this will not be presented here. The measurement vector is

$$y[n] = \begin{bmatrix} y^1[n] & y^2[n-d] \end{bmatrix}^T \tag{4.27}$$

$$y^1[n] = \begin{bmatrix} x_m^1[n] & f_h^1[n] & \cdots & x_m^m[n] & f_h^m[n] \end{bmatrix}^T \tag{4.28}$$

$$y^2[n-d] = \begin{bmatrix} \frac{1}{m}\sum_{i=1}^{m} x_m^i[n-d] - \alpha_p x_t[n-d] \\ \sum_{i=1}^{m} f_s^i[n-d] \\ \frac{1}{m}\sum_{i=1}^{m} x_m^i[n-d] - x_{vt}[n-d] \\ v_{vt}[n-d] \end{bmatrix} \tag{4.29}$$

where d is the communication latency in number of sample times and f_s^i is the reaction force from the tool. These observations are generated based on the actual sensors' readings $x_m^i[n]$, $f_h^i[n]$, $x_t[n]$, and $f_s^i[n]$ (see Figure 4.2). The measurement vector in (4.27) is particularly suited for the LQG design as it contains the delayed tracking errors. The delayed measurements will eventually be incorporated into the system states as will be seen shortly. Note that the slave measurements are delayed by d samples. The rationale is obvious in the case of the slave measurements as the controller is implemented at the master side and it would take d samples before that the slave information arrive at the master end. The virtual tool observations $x_{vt}[n-d]$, and $v_{vt}[n-d]$ which are produced by the control algorithm are also delayed since they depend on the environment force $f_e[n-d]$.

Part of the observation vector in (4.27), i.e. $y^2[n-d]$ can not be directly written in terms of the system's states and inputs in (4.18) and (4.22) due to the existence of the delay. Nonetheless, the treatment of the problem in the discrete-time domain allows for the incorporation of time delay via a finite number of states into the system's model. The delayed measurement vector is produced by passing the original non-delayed signals through d unit delay blocks. The outputs of the unit delay blocks are added to the system's states. The non-delayed observation vectors $y^1[n]$ and $y^2[n]$ can be written in terms of the states and the control actions in

(4.18)-(4.23),

$$y^1[n] = C^1X[n] + D^1u[n] + H^1w[n] + v^1[n] \tag{4.30}$$

$$y^2[n] = C^2X[n] + D^2u[n] + H^2w[n] + v^2[n] \tag{4.31}$$

where $v^1[n]$ and $v^2[n]$ are measurement noise; $X[n]$, $u[n]$, and $w[n]$ have been introduced before. The new augmented state vector is given by

$$X_n[n] = \begin{bmatrix} X[n]^T & y^2[n-1]^T & \cdots & y^2[n-d]^T \end{bmatrix}^T \tag{4.32}$$

and the corresponding system matrices are

$$A_n = \begin{bmatrix} A & 0 & 0 & \cdots & 0 \\ C^2 & 0 & 0 & \cdots & 0 \\ 0 & I & 0 & \cdots & 0 \\ \vdots & & & & \vdots \\ 0 & \cdots & \cdots & I & 0 \end{bmatrix}, \; B_n = \begin{bmatrix} B \\ D^2 \\ 0 \\ \vdots \\ 0 \end{bmatrix} \tag{4.33}$$

$$C_n = \begin{bmatrix} C^1 & 0 & \cdots & 0 \\ 0 & \cdots & 0 & I \end{bmatrix}, \; D_n = \begin{bmatrix} D^1 \\ 0 \end{bmatrix} \tag{4.34}$$

$$G_n = \begin{bmatrix} G & 0 \\ H^2 & I \\ 0 & 0 \\ \vdots & \vdots \\ 0 & 0 \end{bmatrix}, \; H_n = \begin{bmatrix} H^1 & 0 \\ 0 & 0 \end{bmatrix} \tag{4.35}$$

Also, the new process and measurement noise vectors are $w_n[n] = \begin{bmatrix} w[n]^T & v^2[n]^T \end{bmatrix}^T$ and $v_n[n] = \begin{bmatrix} v^1[n]^T & 0 \end{bmatrix}^T$. The input and output remain unchanged, i.e. $u[n]$, and $y[n]$. The master and slave control actions are subject to time delay as well. The delays for the master and slave control signals are one and d samples, respectively.

$$u[n] = \begin{bmatrix} f_{cm}[n]^T & f_{cs}[n] \end{bmatrix}^T = \begin{bmatrix} u^1[n-1]^T & u^2[n-d] \end{bmatrix}^T \tag{4.36}$$

The delay in control signals can be included in the model by augmenting the states as follows

$$\bar{X}[n] = \begin{bmatrix} X_n[n]^T & u^1[n-1]^T & u^2[n-d] & u^2[n-d+1] & \cdots & u^2[n-1] \end{bmatrix}^T \tag{4.37}$$

The new system matrices are

$$\bar{A} = \begin{bmatrix} A_n & B_n^1 & B_n^2 & 0 & 0 & \cdots & 0 \\ 0 & 0 & 0 & 0 & 0 & \cdots & 0 \\ 0 & 0 & 0 & 1 & 0 & \cdots & 0 \\ 0 & 0 & 0 & 0 & 1 & \cdots & 0 \\ \vdots & & & & & & \vdots \\ 0 & \cdots & & & & & 0 \end{bmatrix}, \bar{B} = \begin{bmatrix} 0 & 0 \\ 1 & 0 \\ 0 & 0 \\ 0 & 0 \\ \vdots & \vdots \\ 0 & 1 \end{bmatrix} \tag{4.38}$$

$$\bar{C} = \begin{bmatrix} C_n & D_n^1 & D_n^2 & 0 & \cdots & 0 \end{bmatrix}, \bar{D} = 0 \tag{4.39}$$

$$\bar{G} = \begin{bmatrix} G_n \\ 0 \\ \vdots \\ 0 \end{bmatrix}, \bar{H} = H_n \tag{4.40}$$

The new input vector is

$$\bar{u}[n] = \begin{bmatrix} u^1[n]^T & u^2[n] \end{bmatrix}^T \tag{4.41}$$

and output, process noise, and measurement noise are not changed.

The operator's exogenous force $f_h^{*i}[n]$ is part of the disturbance vector $w_n[n]$. This signal can be modelled by a stochastic process and added to the system's states. This approach would enable the real-time estimation of the force based on the sensory observations. A first-order model is used for the operator's exogenous

force:

$$f_h^{*i}[n+1] + \alpha_{fh}^i f_h^{*i}[n] = n_f^i[n] \tag{4.42}$$

where α_{fh}^i is a constant and $n_f^i[n]$ is a white Gaussian sequence. The final discrete-time state-space representation of the system after the augmentation of f_h^* into the state vector is given by

$$X_f[n+1] = A_f X_f[n] + B_f u_f[n] + G_f w_f[n] \tag{4.43}$$

$$y_f[n] = C_f X_f[n] + D_f u_f[n] + H_f w_f[n] + v_f[n] \tag{4.44}$$

where

$$X_f[n] = \begin{bmatrix} \bar{X}[n]^T & f_h^*[n]^T \end{bmatrix}^T \tag{4.45}$$

$$y_f[n] = y_n[n] = \begin{bmatrix} y^1[n]^T & y^2[n-d]^T \end{bmatrix}^T \tag{4.46}$$

$$u_f[n] = \bar{u}[n] = \begin{bmatrix} u^1[n]^T & u^2[n] \end{bmatrix} \tag{4.47}$$

$$w_f[n] = \begin{bmatrix} n_f[n]^T & f_e^*[n] & \tilde{f}_{cm}[n]^T & \tilde{f}_{cs}[n] & v^2[n]^T \end{bmatrix}^T \tag{4.48}$$

$$v_f[n] = v_n[n] = \begin{bmatrix} v^1[n]^T & 0 \end{bmatrix}^T \tag{4.49}$$

$$n_f[n] = \begin{bmatrix} n_f^1[n] & \cdots & n_f^m[n] \end{bmatrix}^T \tag{4.50}$$

The system matrices are

$$A_f = \begin{bmatrix} \bar{A} & \bar{G}(:, 1:m) \\ 0 & -\alpha_{fh} \end{bmatrix}, \; B_f = \begin{bmatrix} \bar{B} \\ 0 \end{bmatrix} \tag{4.51}$$

$$C_f = \begin{bmatrix} \bar{C} & \bar{H}(:, 1:m) \end{bmatrix}, \; D_f = \bar{D} \tag{4.52}$$

$$G_f = \begin{bmatrix} 0 & \bar{G}_{1\ m+1} & \cdots & \bar{G}_{1\ 2m+4} \\ \vdots & \cdots & \vdots & \\ 0 & \bar{G}_{4m+5d+4\ m+1} & \cdots & \bar{G}_{4m+5d+4\ 2m+6} \\ I & 0 & \cdots & 0 \end{bmatrix} \tag{4.53}$$

$$H_f = \begin{bmatrix} 0 & \bar{H}_{1\ m+1} & \cdots & \bar{H}_{1\ 2m+6} \\ \vdots & & \vdots & \\ 0 & \bar{H}_{2m+2\ m+1} & \cdots & \bar{H}_{2m+4\ 2m+6} \end{bmatrix} \tag{4.54}$$

where $\bar{G}(:, 1:m)$ and $\bar{H}(:, 1:m)$ denote the first m columns of $\bar{G}$ and $\bar{H}$ matrices, respectively and α_{fh} is a diagonal matrix with diagonal elements of α_{fh}^i.

4.3.2 Rigid Contact

When the tool is in rigid contact, the continuous-time dynamics of the slave side are governed by (4.6) with their discrete-time equivalent given in (4.16). Note that the slaves/tool position in rigid contact is modelled by

$$x_t[n+1] = \beta x_t[n] + w_{xs}[n] \tag{4.55}$$

with $\beta \rightarrow 1^-$ and $w_{xs}[n]$ is a white Gaussian sequence. In this case, the vector of discrete states including the master and slave subsystems is chosen as

$$X[n] = \begin{bmatrix} X_m^1[n]^T & \cdots & X_m^m[n]^T & X_s[n]^T \end{bmatrix}^T \tag{4.56}$$

where

$$X_m^i[n] = \begin{bmatrix} \sum_{k=1,\neq i}^m [h_{m_k}^i (x_m^i[n] - x_m^k[n])] + h_s^i (x_m^i[n] - \alpha_p x_t[n]) & v_m^i[n] \end{bmatrix}^T \tag{4.57}$$

$$X_s[n] = \begin{bmatrix} x_t[n] & f_e[n] \end{bmatrix}^T \tag{4.58}$$

and the measurement vector is

$$y[n] = \begin{bmatrix} y^1[n]^T & y^2[n-d]^T \end{bmatrix}^T \tag{4.59}$$

$$y^1[n] = \begin{bmatrix} x_m^1[n] & f_h^1[n] & \cdots & x_m^m[n] & f_h^m[n] \end{bmatrix}^T \tag{4.60}$$

$$y^2[n-d] = \begin{bmatrix} \frac{1}{m} \sum_{i=1}^m x_m^i[n-d] - \alpha_p x_t[n-d] & \sum_{i=1}^m f_h^i[n-d] - \alpha_f f_e[n-d] \end{bmatrix}^T \tag{4.61}$$

where α_f is force scale factor. This leads to a discrete-time difference equation similar to the one in (4.21). The steps to incorporate the delay in the measurements and the control signals as well as the operator's exogenous force $f_h^*[n]$ into the system's states are similar to those in the previous case and will not be repeated here. The dynamics of the augmented system in the discrete-time domain can be

expressed by the following difference equations

$$X_r[n+1] = A_r X_r[n] + B_r u_r[n] + G_r w_r[n] \tag{4.62}$$

$$y_r[n] = C_r X_r[n] + D_r u_r[n] + H_r w_r[n] + v_r[n] \tag{4.63}$$

with

$$X_r[n] = [X[n]^T\ y^2[n-1]^T\ \cdots\ y^2[n-d]^T\ u^1[n-1]^T \tag{4.64}$$

$$u^2[n-d]\ \cdots u^2[n-2]\ f_h^*[n]^T]^T \tag{4.65}$$

$$y_r[n] = y[n] \tag{4.66}$$

$$w_r[n] = \begin{bmatrix} n_f[n]^T & \tilde{f}_{cm}[n]^T & \tilde{f}_{cs}[n] & w_{xs}[n] & v^2[n]^T \end{bmatrix}^T \tag{4.67}$$

$$v_r[n] = \begin{bmatrix} v^1[n]^T & 0 \end{bmatrix}^T \tag{4.68}$$

It should be noted that the one sample delay in the slave control action has already been added to $X_r[n]$ in (4.56).

4.3.3 LQG Control Design

The system dynamics and measurement equations in (4.43)-(4.44) for free motion/soft contact and in (4.62)-(4.63) for rigid contact are in the standard form for the application of the LQG control synthesis. The deterministic inputs to the system are the master and slave control signals; $u_f[n]$, $u_r[n]$. The system is also perturbed by the stochastic inputs $w_f[n]$, $w_r[n]$ which are assumed zero mean white Gaussian sequences. The measurement noise vectors $v_f[n]$, $v_r[n]$ are also zero mean white Gaussian signals. The LQG controller attempts to minimize the effect of the

stochastic disturbance inputs on the states through minimizing the following loss function for $N \rightarrow \infty$ [72]

$$J(u) = \frac{1}{N} E\{\sum_{n=1}^{N} X[n]^T Q X[n] + u[n]^T R u[n] + 2X^T[n]\Gamma u[n]\} \tag{4.69}$$

where $E\{.\}$ denotes the expected value, and $Q \geq 0$, $R > 0$, and $Q - \Gamma R^{-1}\Gamma^T \geq 0$ but here we assume $\Gamma = 0$. The optimal controller is a combination of a constant state feedback gain obtained from solving the corresponding deterministic optimal Linear Quadratic (LQ) control and an optimal *Kalman* filter state estimator, i.e.

$$u[n] = -K\hat{X}[n|n-1] \tag{4.70}$$

where the feedback gain K is given by

$$K = \left(B^T S B + R\right)^{-1} \left(B^T S A + \Gamma^T\right) \tag{4.71}$$

and S is the solution to the following Discrete-time Algebraic *Riccati* Equation (DARE)

$$A^T S A - S - (A^T S B + \Gamma)(B^T S B + R)^{-1}(B^T S A + \Gamma^T) + Q = 0 \tag{4.72}$$

The state estimate $\hat{X}[n|n-1]$ is the output of a *Kalman* filter with the following dynamics

$$\hat{X}[n+1|n] = A\hat{X}[n|n-1] + Bu[n] + L(y[n] - C\hat{X}[n|n-1] - Du[n]) \tag{4.73}$$

The *Kalman* filter gain L is computed as follows

$$L = APC^T \left(\Pi + CPC^T\right)^{-1} \tag{4.74}$$

where P is the solution to the following DARE

$$APA^T - P - APC^T \left(\Pi + CPC^T\right)^{-1} CPA^T + W \tag{4.75}$$

and $W = E\left\{Gw[n]w[n]^T G^T\right\}$ and $\Pi = E\left\{v[n]v[n]^T\right\}$ are the covariances of the process and measurement noise, respectively. Certain conditions must be satisfied for the existence of a solution to the LQG problem. These include the stabilizability of pair (A, B) and detectability of pair (C, A) among others. It can be shown that the teleoperation system satisfies all necessary requirements.

The special form of the system states for free motion/soft contact and the rigid contact facilitates the LQG design for achieving the teleoperation performance objectives. The sensor measurements are the master and slave positions as well as the hand and environment forces. Delayed hand and environment force signals are used to generate delayed virtual tool position and velocity. These synthesized observations along with the actual transformed/delayed observations enter the mode-based LQG controller blocks at the master site which in turn produce the master and slave mode-based control signals using the algorithms described above. The switching logic located at the slave side, uses the sensory information to identify the mode of operation and sends the result back to the controller at the master side. This information is utilized to select the pair of control signals to The control be transmitted to the master and slave actuators (see Figure 4.2).

It should be noted that there is redundancy in the slaves' control signals as the output of the LQG synthesis is $\sum_{i=1}^{m} f_{cs}^{i}[n]$. In general,

$$F_{cm}[n] = \begin{bmatrix} f_{cs}^{1}[n] & \cdots & f_{cs}^{m}[n] \end{bmatrix}^{T} = J_I{}^{\dagger}(\sum_{i=1}^{m} f_{cs}^{i}[n]) + F_{int} \tag{4.76}$$

where $J_I = \begin{bmatrix} 1 & \cdots & 1 \end{bmatrix}$, $\dagger$ denotes the pseudo-inverse and F_{int} is an internal force component that does not contribute to the combined motion of the slaves and tool. The internal force F_{int} can help maintain the contact between the slave manipulators and the tool if the end-effectors are not equipped with grippers.

Remark 4.1: The quadratic terms in $X_f[n]^T Q_f X_f[n]$ and $X_r[n]^T Q_r X_r[n]$ involve position and force tracking errors at concurrent sample times. Therefore despite the presence of $2d$ samples round trip delay, the controller attempts to produce non-delayed position and force tracking. Intuitively, this is achieved through the prediction of master and slave motions by model-based *Kalman* filters. Also, the matrices Q_f and Q_r are positive semi-definite as opposed to positive definite. Therefore, only the tracking errors are penalized in (4.69) and the gains corresponding to the rest of the states in Q's are set to zero. This is critical for the design of the teleoperation controller since the master/slave system must be allowed to move freely in response to operator's input force.

Remark 4.2: The disturbance terms in the model, in particular $f_h^*[n]$ and $f_e^*[n]$, can introduce tracking errors and hence degrade the performance. The effect of these disturbances can be attenuated by tightening the feedback loops through increasing Q and/or decreasing R in (4.69). However, large feedback gains can amplify

the noise and reduce the system's stability margins. The inclusion of $f_h^*[n]$, and similarly $f_e^*[n]$ if needed, in the state vector through the first-order model (4.42) can enhance the performance as it allows for the real-time estimation of $f_h^*[n]$. Nevertheless, such model may not accurately predict the operator's exogenous force for a long prediction horizon. More complex force generation models can be employed to further increase the prediction horizon of the controller.

Remark 4.3: Models of operator, master robot, slave robot, and environment dynamics are used by controller. While the master and slave parameters are often known and constant, the operator and environment dynamics are usually unknown and time-varying. The controllers are designed based on the nominal values of the operator and environment parameters. Variation in these parameters can degrade the performance and may even cause instability. Nevertheless, the results of simulations and analysis presented later demonstrate that a careful selection of the LQG design parameters can render the system sufficiently robust w.r.t. operator and environment parameter changes.

Remark 4.4: Multi-model estimation techniques [74, 76, 77] can be employed to identify the mode of operationbased on sensory observations. Special care should be taken to attain a smooth transition between the mode-based controllers. to this end a simple switching strategy will be introduced later. It is generally difficult to analytically prove the stability of such switching control systems although different approaches have been proposed in the literature [78, 79]. This will remain a subject of future research.

Remark 4.5: The order of controller is equal to the system's order, i.e. $4m+5d+4$ for

free motion/flexible contact and $3m+3d+2$ for rigid contact. The number of sample delays d depends on the control frequency and the communication latency and can become large in some applications. However, it turns out that the controller possesses a sparse structure that can be exploited for its efficient implementation, if needed. It is also possible to adopt a multi-rate control strategy where the teleoperation controller runs at a slower rate than that of the local feedback linearizing controllers.

Remark 4.6: The proposed control approach can be employed in case of time-varying delay by introducing buffers that store measurement and control signals at the master and slave ends. Time-delay is rendered constant by adding artificial delay to these signals if and when necessary. Nevertheless, such an approch would be conservative since the control is designed for the maximum delay.

Chapter 5

Simulation and Experimental Results

The proposed control algorithms for cooperative teleoperation are evaluated through simulation and experiment in this chapter.

5.1 Case Study

This section presents a numerical design example to demonstrate the effectiveness of the proposed control algorithms. A single-axis linear two-master/two-slave system is considered as illustrated in Figure 5.1. This example is based on the experimental setup that will be introduced later. The dynamics of human operators, master robots, slave robots, and the tool are modelled by linear mass-spring-damper systems with impedances of the form $ms + b + k/s$. The single-axis tool frame is located at the contact point between tool and environment. The parameters used in the simulations reflect those of the actual experimental setup.

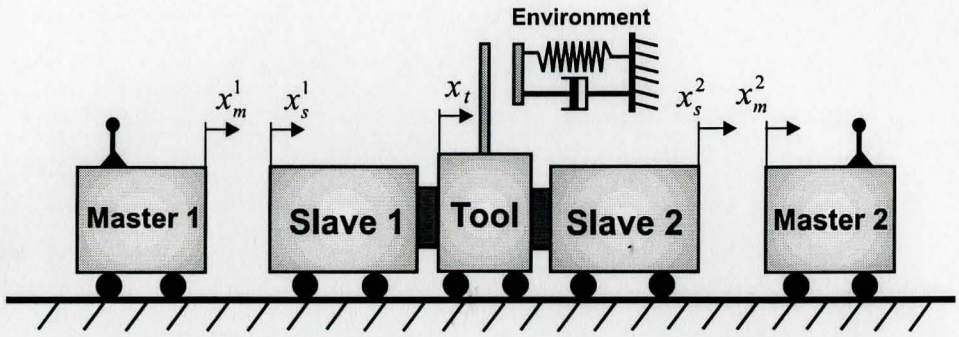

Figure 5.1: The schematic of the linear one-axis two-master/two-slave teleoperation system.

System parameters:

$$
\begin{array}{lll}
m_m^1 = m_m^2 = 0.5kg & b_m^1 = b_m^2 = 0.5N.s/m & k_m^1 = k_m^2 = 0.1N/m \\
m_s^1 = m_s^2 = 3.5kg & b_s^1 = b_s^2 = 6N.s/m & k_s^1 = k_s^2 = 0.1N/m \\
m_t = 0.82kg & b_t = 2N.s/m & k_t = 0.01N/m \\
m_h^1 = m_h^2 = 0.35kg & b_h^1 = b_h^2 = 0.1N.s/m & k_h^1 = k_h^2 = 0.02N/m
\end{array}
$$

All values are expressed in the metric units.

5.2 Simulation Results

5.2.1 Discrete-Time LQG Controller

The proposed LQG control scheme of Chapter 3 is applied to the single-axis two-master/two-slave system of the previous section. The controller is implemented at the master side. The operators manipulate the slave robots in free motion and in contact with a rigid environment. Two different controllers are designed. The first controller is intended for free motion operation and the second controller handles

rigid contact.

Controller Switching:

The switching logic used in the simulations is simple. While in free motion, the controller enters the rigid mode if the magnitude of the environment force surpasses a predefined threshold. However, this force is not available directly. A disturbance observer is employed to estimate it based on measurements of contact forces between the slaves and the tool. The force observer will be explained later. To return to the free motion mode, the average slave velocity over a short window of time and the operator's measured force in the direction away from the contact must be below and above small predefined thresholds. Such logic will eliminate the possibility of erroneous switching due to the bouncing against the rigid environment during the transition period. Also, the number of free-to-rigid bounces may be reduced simply by adding extra damping to the slave controller during the transition period.

The controller performance and its robustness w.r.t. parameter variations are examined through various simulation scenarios. These include teleoperation under different communication delays with matched and mismatched parameters. Delay is introduced in the slave position and force information as well as the slave control signal since the controller is implemented at the master end.

The system and controller parameters used in the simulations are given below.

System parameters:

$$\begin{array}{lll} m_{vt} = 3kg & b_{vt} = 2N.s/m & k_{vt} = 0.01N/m \\ m_e = 0.01kg & b_e = 1N.s/m & k_e = 0.1N/m \\ \alpha_f = 1kg & \alpha_p = 1 & \alpha^i_{fh} = \beta = 0.999 \end{array}$$

LQG parameters:

$$R = diag(0.05, 0.05, 0.05)$$

$$E\{ww^T\} = diag(0.25, 0.25, 0.01, 0.01, 0.01, 10^{-8}, 10^{-4})$$

$$E\{vv^T\} = diag(10^{-8}, 10^{-4}, 10^{-8}, 10^{-4}, 0, 0)$$

$$q^f_{1i} = \begin{cases} 10^3 & i = d \\ 0 & \text{otherwise} \end{cases} \qquad q^f_{2i} = \begin{cases} 10^2 & i = d \\ 0 & \text{otherwise} \end{cases}$$

$$q^r_{1i} = \begin{cases} 10^4 & i = d \\ 0 & \text{otherwise} \end{cases} \qquad q^r_{2i} = \begin{cases} 1 & i = d \\ 0 & \text{otherwise} \end{cases}$$

The sampling frequency is $128Hz$ for the LQG controller and $1024Hz$ for local controllers. According to *sampling theorem,* for fully reconstruction of a band-limited signal, the sampling frequency must be at least twice as large as the highest frequency component of the original signal [80, 81]. In control loops the sampling rate should be about twenty times larger than the highest frequency component. There will be abrupt changes in force signals when a transition happens from free

motion to rigid contact and such sharp changes contain high frequency components. Therefore, for stability reasons the sampling rate should be high when we have force feedback. Since the state vector contains delayed control and measurement signals, the dimension of the state vector will increase with increasing the sampling frequency. Thus the sampling frequency of the LQG controller was chosen to be smaller than that of the local controllers.

Simulation with Matched Parameters

In this case, the system parameters used in the LQG design are the same as those employed to simulate master, slave, and environment dynamics. Three different levels of round trip time delay are examined, i.e. 125ms, 250ms, and 500ms. Figure 5.2 shows the position and force tracking results. The LQG controller demonstrates excellent position tracking and impedance shaping in free motion. Note that the positions of masters and slave closely follow that of the virtual tool without delay. The controller uses the model information to compensate for the delay through prediction. The tracking error slightly increases as latency becomes larger. This demonstrates the effect of uncertainties such as the operator's exogenous force and measurement noise on the system's performance.

The controller exhibits stable contact transition from free motion to rigid contact and vise versa. There is a delay in force tracking during the rigid contact. This is due to the fact that first-order model for operator's exogenous force f_h^* in (4.42) can not accurately predict its behavior. The operators perceive a rigid contact despite a small discrepancy between masters and slaves positions. This is evident from the master position profiles which show constant master positions despite

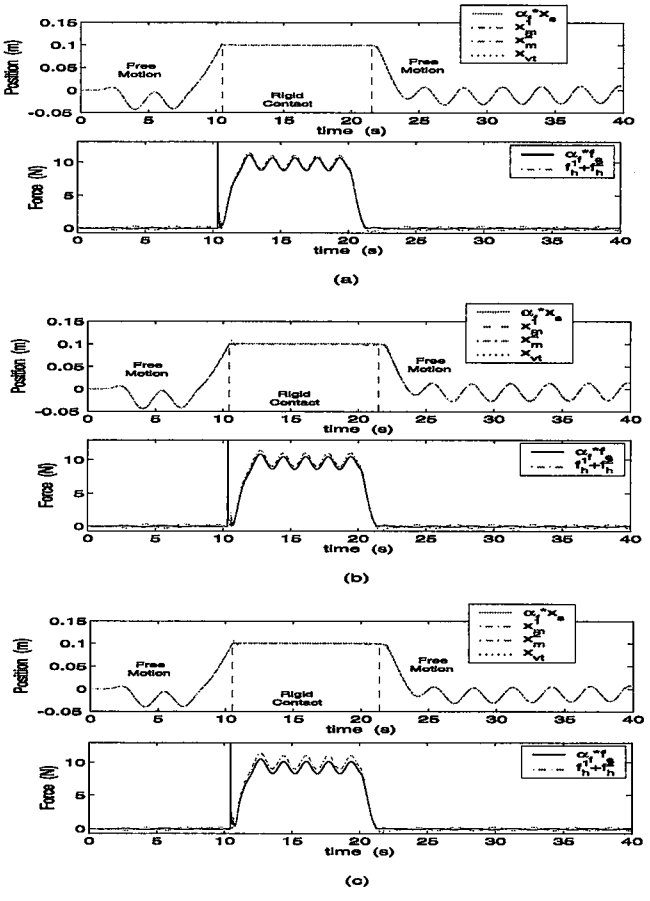

Figure 5.2: LQG Position and force tracking for matched parameters: (a) 125ms delay (b) 250ms delay (c) 500ms delay.

the variations in the applied hand forces. The force oscillation in the rigid contact is due to the operators' deliberate force and is intended to display the force tracking capability of the controller.

Simulation with Mismatched Parameters

The simulations were repeated, this time with mismatched parameters. The master and slave parameters can be estimated with high accuracy. The design example

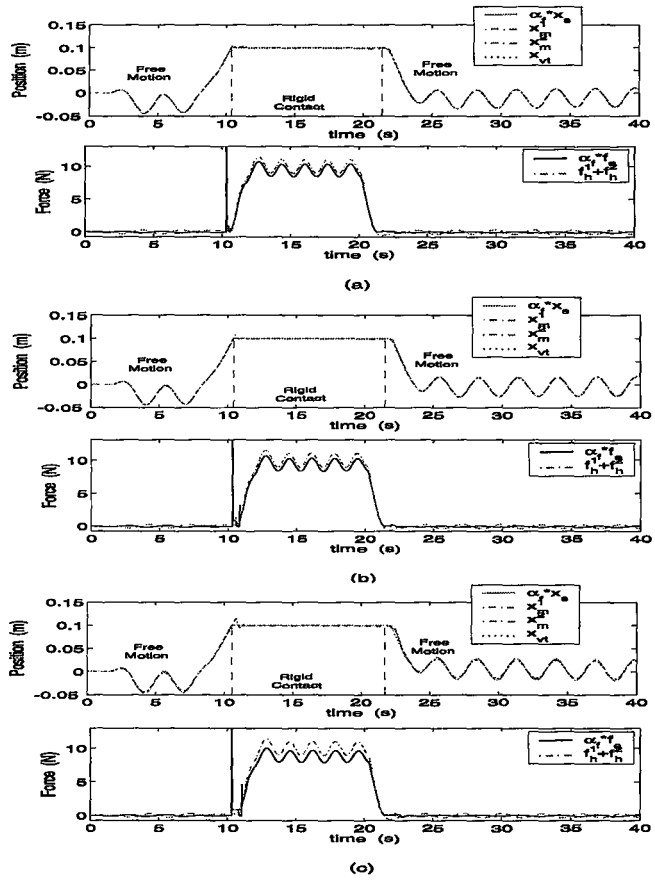

Figure 5.3: LQG Position and force tracking for mismatched model parameters: (a) 125ms delay (b) 250ms delay (c) 500ms delay.

requires no environment parameter as it considers free motion and rigid contact. However, the arm parameters are unknown and can vary from one operator to another. Figure 5.3 displays the results for the case in which m_h(real)= 1.0kg and m_h(model)= 0.35kg. Figure 5.4 displays the results for the case in which m_h(real)= 0.05kg and m_h(model)= 0.35kg. The LQG controller still demonstrates accurate force and position tracking with stable contact behavior for all three levels of time delay despite the large parameter mismatch as is evident in this figure.

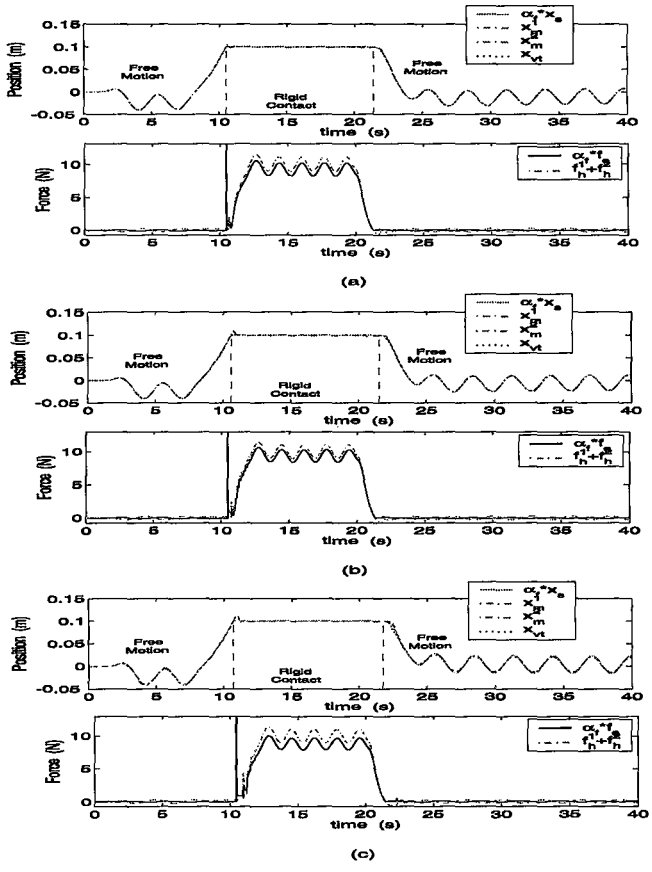

Figure 5.4: LQG Position and force tracking for mismatched model parameters: (a) 125ms delay (b) 250ms delay (c) 500ms delay.

Robust Stability Analysis

The proposed multiple-model LQG controller is a model-based approach that requires the parameters of master, slave, operator, and the environment (in soft contact). The robustness of the controller was demonstrated through a few numerical simulation scenarios in the previous section. It is also possible to investigate this robustness via classical linear analysis tools such as the *Nyquist* theorem. To avoid complications of a multi-variable analysis, we study the robustness with respect to

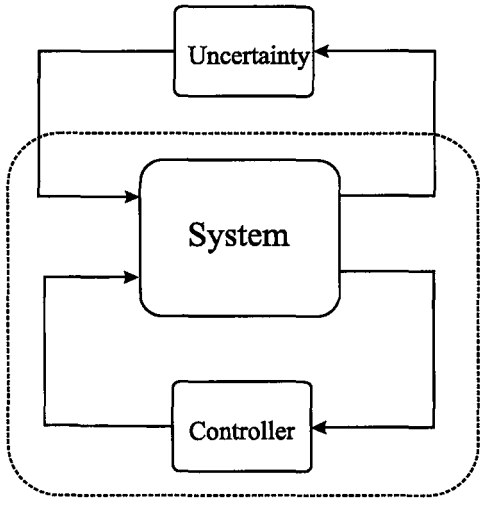

Figure 5.5: System structure for Nyquist stability analysis.

changes in individual parameters separately. In each case, the controller/observer and all system parameters are fixed except one parameter of interest. The *Nyquist* analysis is then employed to obtain the value of parameter for which the system becomes marginally stable [82,83]. The system structure for *Nyquist* stability analysis is shown in Figure 5.5, where the closed loop system can be considered as a single-input/single-output (SISO) system. In the following the robustness analysis is applied to the single-axis linear two-master/two-slave bilateral teleoperation system of Figure 5.1.

Robustness against mismatch in environment stiffness

The environment stiffness in the design of the free motion controller was assumed 0.1N/m. The free motion controller could also be used to interact with soft environments. Obviously, this will introduce uncertainty in the form of environment stiffness in the system's dynamics. In Figure 5.6(a), the maximum allowable environment stiffness for the controller with the above parameters is plotted as a

function of the time delay. The maximum stiffness decreases by the amount of time delay from over 11000N/m for delays around 15ms to about 400N/m for a delay of 250ms. It should be noted that the same controller has been used to produce the results for different delays. The controller parameters can always be adjusted to balance the performance and robust stability based on the value of the delay and the application requirements. Alternatively by designing separate controllers for free motion and soft contact, system's performance and stability can be both enhanced in the expense of having a more complex controller.

Robustness against mismatch in arm mass and environment stiffness

The sensitivity of the free motion controller with respect to simultaneous variations in the operator's arm mass and the environment stiffness was also analyzed for a time delay of 125 ms. The results are given in Figure 5.6(b) where the maximum allowable environment stiffness is plotted for different values of actual arm mass. According to this figure, the maximum stiffness for the free motion controller decreases as the actual arm mass increases.

Robustness against mismatch in arm mass for rigid contact controller

The arm mass is the critical parameter in the design of the rigid contact controller. The robust stability of the controller w.r.t. variations in this parameter is demonstrated in Figure 5.6(c) where that maximum allowable arm mass is plotted as a function of communication delay. Again, the arm mass value used in the design is $m_h = 0.35$kg.

In summary, it can be concluded that the designed controller is fairly robust with respect to the uncertainties considered in the analysis. Obviously, it is difficult to specify objective targets for the controller robustness margins. The designer

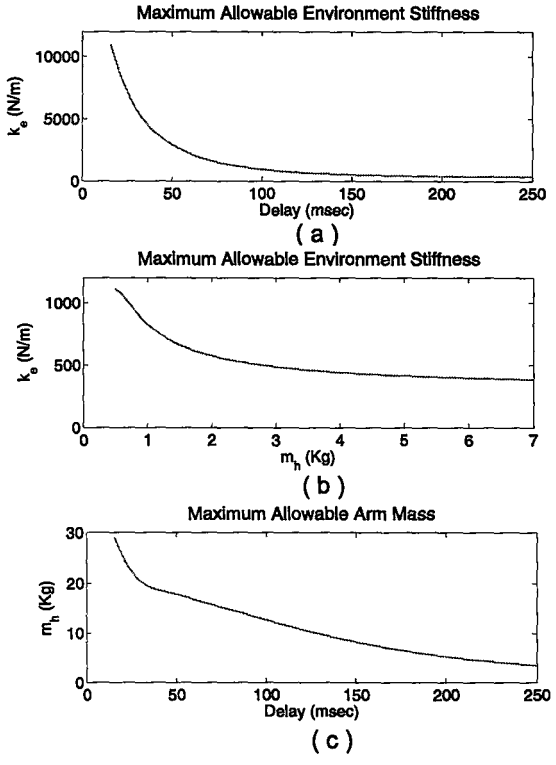

Figure 5.6: (a) Robustness of free motion LQG controller w.r.t. mismatch in environment stiffness ($k_e = 0.1$ in design). (b) Robustness of free motion LQG controller w.r.t. mismatch in arm mass and environment stiffness ($m_h = 0.35$ and $k_e = 0.1$ in design). (c) Robustness of rigid contact LQG controller w.r.t. mismatch in arm mass ($m_h = 0.35$ in design).

should set the performance and robustness goals based on the application requirements and then tune the controller design parameters to achieve those objectives, if possible.

5.2.2 Adaptive Nonlinear Controller

The proposed adaptive nonlinear control scheme of Chapter 3 is applied to the single-axis two-master/two-slave system. In this case

$$\Psi(x_s^1) = x_s^1 \qquad \Psi(x_s^2) = x_s^2$$

and hence $J_t = \begin{bmatrix} 1 & 1 \end{bmatrix}$. Similarly for the masters

$$\Phi(x_m^1) = x_m^1 \qquad \Phi(x_m^2) = x_m^2$$

Controller parameters are: $C = 24\pi$, $\Lambda = 20$, $A = 0.0025$, $K_s = 100$, $K_m^i = 100$ for $i = 1, 2$. All values are expressed in the metric system of units. The sampling frequency is $1024Hz$, and the force and position scaling factors are $K_f = 4$ and $K_p = 1$, respectively. This generates a virtual mass of 1.33kg and damping of 26.5Ns/m.

The redundancy in slaves' has been used to control the internal force exerted on the tool according to (3.25) with $f_{int}^d = 20$N. This assists in keeping the contact with the tool during the operation as slaves are not equipped with a gripper mechanism. Force measurement noise and encoder quantization errors are included in the simulation.

The proposed controller requires the measurement of environment force f_e. However, this is not available in our experimental setup. Instead, the contact forces between the slaves and the tool are measured through two sensors. In stable rigid contact, the environment force can be directly computed from the force sensors'

readings as the tool velocity and acceleration are zero. Nevertheless, the environment reaction force must be estimated for flexible contact. A disturbance observer has been designed and implemented to estimate this force [84]. The observer dynamics are governed by

$$\begin{aligned} \dot{x}_o^1 &= x_o^2 + \tfrac{k_{vo}}{m_t}(x_t - x_o^1) \\ \dot{x}_o^2 &= \tfrac{1}{m_t}\left[-b_t\dot{x}_t - k_t x_t + k_{po}(x_t - x_o^1) + f_t^1 + f_t^2\right] \end{aligned} \tag{5.1}$$

where x_o^1 and x_o^2 are the observer states, and k_{po} and k_{vo} are the observer gains. f_t^1 and f_t^2 are the force sensors' measurements. Using the above dynamics and the dynamics of the tool,

$$m_t\ddot{x}_t + b_t\dot{x}_t + k_t x_t = f_t^1 + f_t^2 + f_e \tag{5.2}$$

it can be easily shown that

$$m_t\dddot{\tilde{x}}_t + k_{vo}\ddot{\tilde{x}}_t + k_{po}\dot{\tilde{x}}_t = \dot{f}_e \tag{5.3}$$

where $\tilde{x}_t = x_t - x_o^1$ is the observer error. The environment force for the frequencies below the bandwidth of the error dynamics can be approximated by

$$f_e \approx k_{po}\tilde{x}_t \tag{5.4}$$

Note that the observer is even useful for rigid contact operation as it can signal a transition from free motion to contact and vise versa. This triggers the rigid contact controller.

The switching terms in masters's control actions have been eliminated by augmenting the master/operator parameters' vector with the operators' intentional forces, f_h^{1*} and f_h^{2*} as explained in Remark 4.4. Simulations were conducted for two different scenarios; first with a flexible environment and then a rigid environment. The results are presented below.

Flexible Environment

The total simulation time is 30 seconds during which the operators cooperatively move the tool from its initial position and make contact with a flexible environment with stiffness of $k_e = 500$. Then, they withdraw the tool and move it in free motion. Finally, the operators make another contact with the flexible environment while applying a sinusoidal force to the master devices. Figure 5.7(a) shows an excellent position tracking between the masters and slaves both in free motion and in contact with the environment.

The sum of the operators' hand forces reflected to the slave side along with the force exerted by the tool on the environment and its estimate by the observer are plotted in Figure 5.7(b). Note that how the environment force tracks the operators' net force when the tool is in contact with the environment. The operators' net force drive the intervening tool dynamics in free motion. The synthesized tool dynamics cause the force discrepancy seen in Figure 5.7(b) when the tool is moved during the contact. The estimated stiffness at the slave side, $k_s^1 + k_s^2 + k_t + \sigma_f k_e$, is depicted in Figure 5.7(c). The controller accurately tracks variations in the environment stiffness as can be observed in the figure.

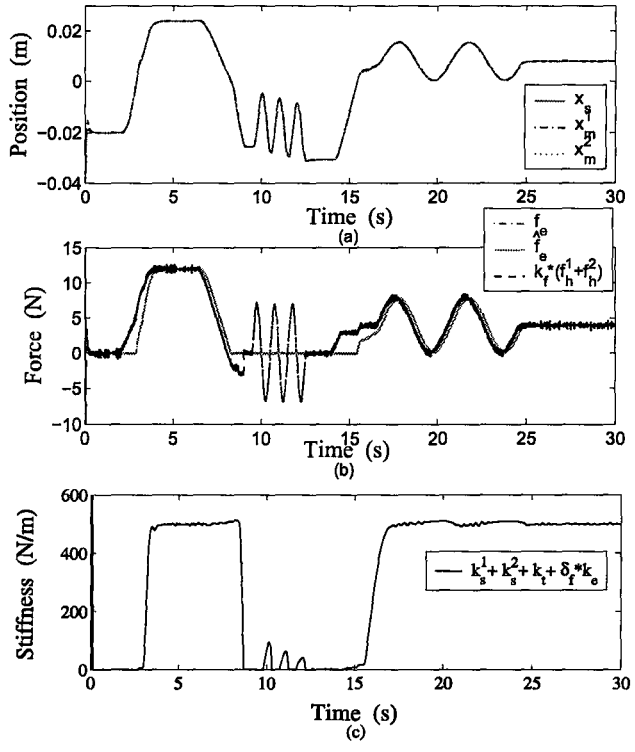

Figure 5.7: Adaptive nonlinear controller simulation results for flexible environment: (a) position tracking (b) force tracking (c) environment's stiffness estimate.

Rigid Environment

A similar scenario was considered to evaluate the performance of the controller for the case of contact with a rigid environment during a simulation period of 16 seconds. In this case, the value of σ_r is determined based on the environment force estimates. Figure 5.8 depicts accurate position and force tracking in free motion and in contact with the rigid environment. The contact behavior is stable and well damped. There is an improvement in the rigid contact force tracking results compared with those of the flexible environment. This is due to lack of motion in rigid contact which eliminates the effect of the synthesized tool dynamics.

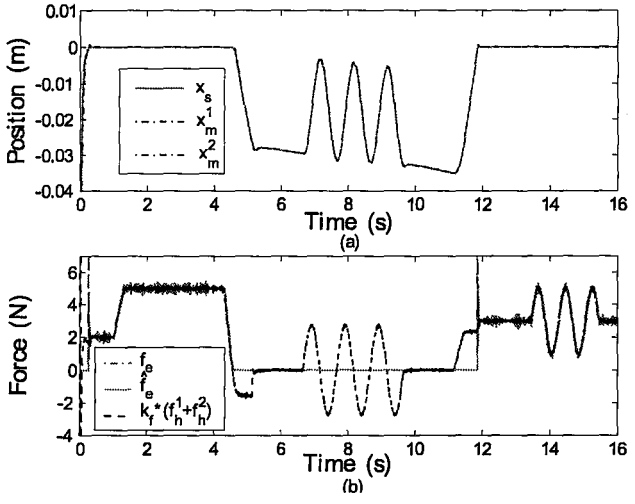

Figure 5.8: Adaptive nonlinear controller simulation results for rigid environment: (a) position tracking, (b) force tracking.

5.3 Experimental Setup

This section presents the results of experimental studies conducted for further evaluation of the proposed adaptive nonlinear cooperative teleoperation scheme. The experimental setup is displayed in Figure 5.9. The two-master/two-slave system is composed of:

(i) A linear track with three moving carts: The two side carts which are the slaves in the experiments, are motorized, and their positions along the track are measured by incremental rotary encoders installed on the motor shafts. The encoders produce 4,096 counts per revolution which approximately yield a 0.01mm linear position measurement resolution. Special care has been taken to reduce backlash in the carts' movements. The Coulomb and viscous friction of the carts are compensated by active control. Two *Mini40* force sensors from *ATI Industrial Automation* have been installed on the carts which measure the interaction force

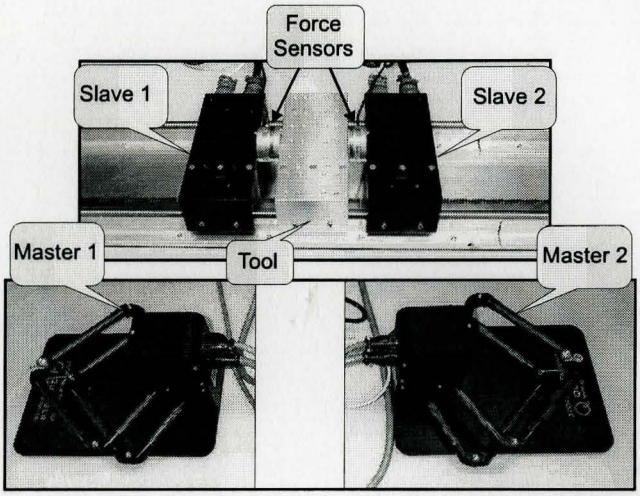

Figure 5.9: The cooperative teleoperation experimental setup.

between the slaves and the tool. The tool is the middle cart in Figure 5.9 and it has been designed such that it can freely move on the track. The motion of the tool is blocked in one direction by a rigid or flexible stop inserted in the middle of the track. This stop cannot be seen in Figure 5.9 as it is hidden under the tool cart.

(ii) Two planar twin pantograph haptic interfaces from *Quanser Consulting* are employed as master robots as shown in Figure 5.9. Each device provides three active degrees of motion, i.e. two translations and one rotation using four electric motors. The motor shaft angles are measured by optical encoders that produce 20,000 counts per revolution. In the experiments, only one axis of motion is required. Therefore, one of the translational and the rotational degrees of freedom are locked using a work-space proportional-derivative controller. The redundancy in actuation of the pantographs is exploited to minimize the norm of required motor torque vector for generating a given work-space force. The control system renders the device into a one-axis haptic interface that is suited for the experiments.

The rigid dynamics of the twin pantograph haptic parallel mechanism are rather complex. Instead, the device is modelled as a position-dependent mass along its axis of motion. The variation in the mass can be handled by the master/operator adaptation law (3.29). No force sensor is installed on master device in order to simplify the mechanical design and also to reduce the mass of the interface. Instead, disturbance observers similar to the one discussed earlier have been designed and implemented to estimate the operators' hand forces [84].

The control algorithm has been implemented using *Matlab Realtime Workshop Toolbox* and *Tornado 2.2/VxWorks 5.4* RTOS by *WindRiver*. The control rate is set to 1024Hz. Q8 multifunction I/O boards by *Quanser Consulting* collect sensory information and output the control commands.

Two sets of experiments were conducted, one with flexible contact and another with rigid contact. In the experiments, two operators cooperatively moved the tool in free motion and made contact with the environment several times. Experiments were repeated with different operators and similar behavior was observed.

5.4 Experimental Results

5.4.1 Adaptive Nonlinear Controller

The redundancy in slaves' has been used to control the internal force exerted on the tool according to (3.25) with $f_{int}^d = 20\text{N}$. This assists in keeping the contact with the tool during the operation as slaves are not equipped with a gripper mechanism.

Flexible Environment

Experimental results for flexible contact are shown in Figure 5.10. The system demonstrates accurate position tracking both in free motion and in contact with the environment. In contact situation, the force exerted on the environment by the tool, tracks the operators' net force after the velocity of the tool approaches zero. This is expected behavior due to the intervening tool dynamics. Also, the adaptive controller is able to estimate the environment stiffness effectively as shown in Figure 5.10(c). The small non-zero stiffness estimates in free motion are most likely due to environment force observation errors.

Rigid Environment

Experimental results for the rigid contact are presented in Figure 5.11. The rigid contact behavior is stable and well damped. The position tracking is accurate both in free motion and in contact phases. The system also demonstrates excellent force tracking between the operators' net force and the environment force when the tool is pushed against the rigid environment.

Experiments have also been conducted using two decoupled four-channel teleoperation systems for performing the same task. The system demonstrated poor contact stability. The operators were mostly unsuccessful in grasping the tool because of contact instability. Even in cases in which the force gains were reduced to improve stability, the contact between the tool and slaves were frequently lost due to poor coordination between the operators. In summary, the cooperative controller provides a superior transparent response in contact with the rigid environment and greatly facilitate the coordination between the operators when compared

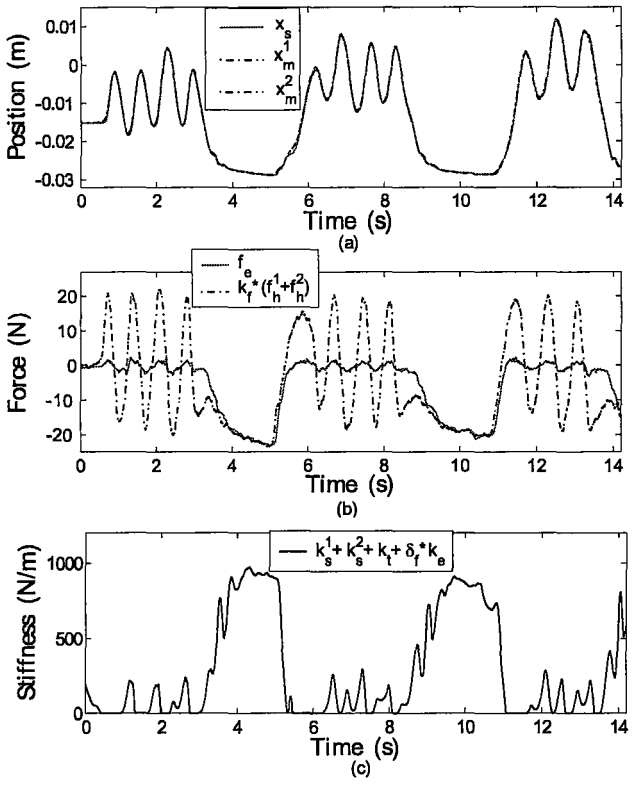

Figure 5.10: Adaptive nonlinear controller experimental results for flexible environment: (a) position tracking (b) force tracking (c) environment's stiffness estimate.

with decoupled single-slave/single-master controllers.

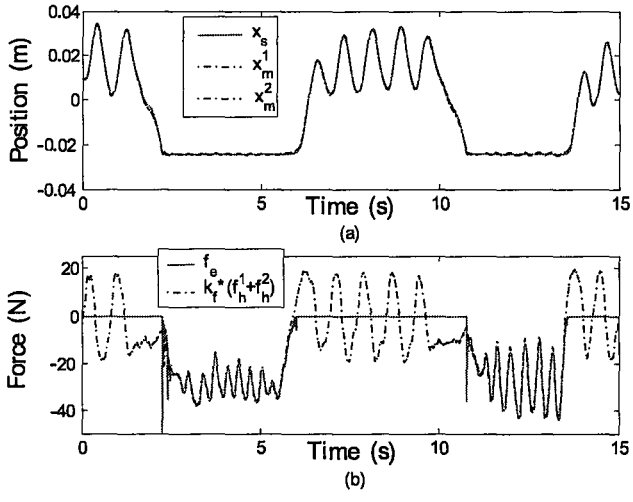

Figure 5.11: Adaptive nonlinear controller experimental results for rigid environment: (a) position tracking (b) force tracking.

Chapter 6

Conclusions and Future Work

This thesis studied the problem of coordinated control of multi-master/multi-slave (MMMS) teleoperation systems. The vast majority of reported work in the literature are concerned with single-master/single-slave (SMSS) teleoperation applications. The few previous reports in cooperative teleoperation either ignore the dynamic interaction of the slaves through the tool or limit their scope to free motion coordination. They also sacrifice transparency objectives in order to gain robust stability in the presence of time delay.

6.1 Contributions of Thesis

Cooperative Teleoperation

A general architecture for cooperative teleoperation control was introduced.

- The proposed framework employs a fully connected communication architecture, which allows for transmission of position and force information between all master and slave robots.
- The dynamics of master and slave manipulators, operators, tool, and environment were incorporated in the model.
- Relevant performance measures were defined to enhance cooperative operation.

Linear and adaptive nonlinear controllers were designed to achieve desired performance as well as to address communication time delay and parametric uncertainty issues.

Adaptive Nonlinear Controller

- The nonlinear dynamics of master and slave manipulators, operators, tool, and environment were incorporated into an adaptive nonlinear control architecture.
- The stability of the closed-loop system in the presence of parametric uncertainty and in contact with flexible and rigid environments was proven through Lyapunov analysis.
- The controller establishes a desired position-position correspondence between masters and slaves. It also provides the operators with a controllable virtual intervening tool impedance.

Discrete-Time LQG Controller

- State space models were developed for various phases of teleoperation that include errors corresponding to non-delayed virtual tool impedance shaping, position tracking, and force tracking.
- Delays in control and measurement signals were also incorporated into these models.
- Model-based output-feedback LQG controllers were designed for free motion/soft contact and contact with rigid environments with switching between the controllers occurring according to the identified mode of operation.
- The Nyquist technique was utilized to analyze the robustness of the controllers with respect to variations in the system's parameters.

Simulation and experimental results demonstrated that the proposed approaches are highly effective in coordinating the operation in a two-master/two-slave single-axis teleoperation setting.

6.2 Directions for Future Research

Functional Differential Equations

As a future work, the nonlinear cooperative teleoperation system can be modelled by functional differential equations [85] instead of ordinary differential equations in order to incorporate the communication time delay explicitly. There is

a relatively rich literature about the control of systems with state delays that are modelled by functional differential equations but without input or output delays [86–88]. Control of a teleoperation system with input and output delays is a much more difficult and challenging problem. Different extensions of control Lyapunov functions to time delay systems have been proposed in the literature such as control Lyapunov-Razumikhin functions (CLRF) and control Lyapunov-Krasovsky functionals (CLKF) [89–91]. Adaptive control laws that guarantee stability could be obtained by these approaches.

Experimental Evaluation of the LQG Controller

The proposed LQG controller should be evaluated experimentally.

Adaptive LQG Controller

Adaptive local nonlinear controllers can be employed to cope with uncertainties and achieve linear dynamic models for master and slave robots [92, 93]. The obtained linear dynamic models can be controlled by the LQG controller.

Decentralized LQG Controller

The proposed LQG controller has a centralized structure and located at the master side in order to obtain better estimates of operators' intentional force. A drawback of the centralized approach is that the slaves' position and force information are not used locally. Extra time delay is introduced in using the slaves' position and force data due to sending the information to the controller at the master side.

Therefore, a decentralized version of this controller has advantage over the centralized one especially in the multi-robot case that operators are at distant positions. Decentralization of the LQG controller, based on the techniques of [94] and [95] and newer methods that consider the time delay issue [96–98], is recommended as a future work.

Bibliography

[1] R. J. Schilling, *Fundamentals of Robotics: Analysis and Control.* Prentice Hall, 1990.

[2] T. B. Sheridan, *Telerobotics, Automation, and Human Supervisory Control.* The MIT Press, 1992.

[3] T. Sheridan, "Telerobotics," *Automatica*, vol. 25, no. 4, pp. 487–507, 1989.

[4] C. Melchiorri and A. Eusebi, "Telemanipulation: system aspects and control issues ," in *Proc. Model. Cont. Mechan. Robot.*, pp. 149–183, 1996.

[5] S. Salcudean, "Control for teleoperation and haptic interfaces," *Control Problems in Robotics and Automation LNCIS230, B. Siciliano and K.P. Valavanis (Eds.). Springer*, pp. 51–66, 1998.

[6] G. Raju, G. Verghese, and T. Sheridan, "Design issues in 2-port network models of bilateral remote teleoperation," in *Proc. IEEE Int. Conf. Robot. Automat.*, pp. 1317–1321, 1989.

[7] B. Hannaford, "A design framework for teleoperators with kinesthetic feedback," *IEEE Trans. Robot. Automat.*, vol. 5, no. 4, pp. 426–434, 1989.

[8] G. Leung, B. Francis, and J. Apkarian, "Bilateral controller for teleoperators with time delay via mu-synthesis," *IEEE Trans. Robot. Automat.*, vol. 11, no. 1, pp. 105–116, 1995.

[9] H. Kazerooni, T. Tsay, and K. Hollerbach, "A controller design framework for telerobotic systems," *IEEE Trans. Contr. Syst. Technol.*, vol. 1, no. 1, pp. 50–62, 1993.

[10] D. Lawrence, "Stability and transparency in bilateral teleoperation," *IEEE Trans. Robot. Automat.*, vol. 9, no. 5, pp. 624–637, 1993.

[11] Y. Yokokohji and T. Yoshikawa, "Bilateral control of master-slave manipulators for ideal kinesthetic coupling-formulation and experiment," *IEEE Trans. Robot. Automat.*, vol. 10, no. 5, pp. 605–620, 1994.

[12] K. Hashtrudi-zaad and S. Salcudean, "Analysis of control architectures for teleoperation systems with impedance/admittance master and slave manipulators," *Int. J. Robot. Res.*, vol. 20, no. 6, pp. 419–445, 2001.

[13] R. Anderson and M. Spong, "Bilateral control of teleoperators with time delay," *IEEE Trans. Automat. Contr.*, vol. 34, no. 5, pp. 494–501, 1989.

[14] G. Niemeyer and J.-J. Slotine, "Stable adaptive teleoperation," *IEEE J. Oceanic Eng.*, vol. 16, no. 1, pp. 152–162, 1991.

[15] P. Arcara and C. Melchiorri, "Control schemes for teleoperation with delay: A comparative study ," *Robotics and Autonomous Systems*, vol. 38, pp. 49–64, 2002.

[16] R. J. Adams and B. Hannaford, "Stable haptic interaction with virtual environments," *IEEE Trans. Robot. Auto.*, vol. 15, pp. 465–474, 1999.

[17] J. Colgate, "Robust impedance shaping telemanipulation," *IEEE Trans. Robot. Automat.*, vol. 9, no. 4, pp. 374–384, 1993.

[18] J. Yan and S. Salcudean, "Teleoperation controller design using H_∞-optimization with application to motion-scaling," *IEEE Trans. Contr. Syst. Technol.*, vol. 45, no. 11, pp. 244–258, 1996.

[19] R. S. H. Istepanian, J. Wu, J. F. Whidborne, J. Yan, and S. E. Salcudean, "Finite word length stability issues of a teleoperation motion-scaling control system," in *Proc. UKACC Int. Conf. Control*, pp. 1676–1681, 1998.

[20] R. S. H. Istepanian, J. Wu, and J. F. Whidborne, "Controller realizations of a teleoperated dual-wrist assembly system with finite word length considerations ," *IEEE Trans. Control Systems Technology*, vol. 9, pp. 624–628, 2001.

[21] Y. Strassberg, A. Goldenberg, and J. Mills, "A new control scheme for bilateral teleoperating systems: Lyapunov stability analysis," in *Proc. IEEE Int. Conf. Robot. Auto.*, pp. 837–842, 1992.

[22] G. M. H. Leung and B. A. Francis, "Robust nonlinear control of bilateral teleoperators," in *Proc. IEEE Int. Conf. Robot. Auto.*, pp. 2119–2123, 1994.

[23] J.-E. Slotine and W. Li, "On the adaptive control of robot manipulators," *Int. J. Robot. Research*, vol. 6, no. 3, pp. 49–59, 1987.

[24] K. Hashtrudi-Zaad and S. Salcudean, "Adaptive transparent impedance reflecting teleoperation," in *Proc. IEEE Int. Conf. Robot. Auto.*, pp. 1369–1374, 1996.

[25] H. K. Lee and M. J. Chung, "Adaptive controller of a master-slave system for transparent teleoperation ," *J. Robotic Systems*, vol. 15, pp. 465–475, 1998.

[26] W.-H. Zhu and S. Salcudean, "Stability guaranteed teleoperation: an adaptive motion/force control approach," *IEEE Trans. Automat. Contr.*, vol. 45, no. 11, pp. 1951–1969, 2000.

[27] J. H. Ryu and D. S. Kwon, "A Novel adaptive bilateral control scheme using similar closed-loop dynamic characteristics of master/slave manipulators ," *J. Robotic Systems*, vol. 18, pp. 533–543, 2001.

[28] N. V. Q. Hung, T. Narikiyo, and H. D. Tuan, "Nonlinear adaptive control of masterslave system in teleoperation ," *Control Engineering Practice*, vol. 11, pp. 1–10, 2003.

[29] C. A. Desoer and M. Vidyasagar, *Feedback Systems: Input-Output Properties*. Academic Press, 1975.

[30] J.-E. Slotine and W. Li, *Applied Nonlinear Control*. New Jersey: Prentice-Hall Inc., 1991.

[31] R. Anderson and M. Spong, "Asymptotic stability for force reflecting teleoperators with time delay," *Int. Journ. Robotics Research*, vol. 11, no. 2, pp. 135–142, 1992.

[32] G. Niemeyer and J. J. E. Slotine, "Telemanipulation with time delays," *Int. Journ. Robotics Research*, vol. 11, no. 2, pp. 873–890, 2004.

[33] S. Stramigioli, A. van der Schaft, B. Maschke, and C. Melchiorri, "Geometric scattering in robotic telemanipulation ," *IEEE Trans. Robot. Auto.*, vol. 18, pp. 588–596, 2002.

[34] N. A. Tanner and G. Niemeyer, "Online tuning of wave impedance in telerobotics," in *Proc. IEEE Int. Conf. Robot. Auto. and Mechatronics*, pp. 7–12, 2004.

[35] N. Chopra, M. W. Spong, and R. Lozano, "Adaptive coordination control of bilateral teleoperators with time delay,," in *Proc. 31st Conf. Decision Cont.*, 2004.

[36] J. H. Ryu, D. S. Kwon, and B. Hannaford, "Stable teleoperation with time-domain passivity control ," *IEEE Trans. Robot. Auto.*, vol. 20, pp. 365–373, 2004.

[37] N. A. Tanner and G. Niemeyer, "Practical limitations of wave variable controllers in teleoperation," in *Proc. IEEE Int. Conf. Robot. Auto. and Mechatronics*, pp. 25–30, 2004.

[38] Y. Yokokohji, T. Imaida, and T. Yoshikawa, "Bilateral control with energy balance monitoring under time-varying communication delay," in *Proc. IEEE Int. Conf. Robot. Auto.*, pp. 2684–2689, 2000.

[39] R. Lozano, N. Chopra, and M. W. Spong, "Passivation of force reflecting bilateral teleoperators with time-varying delay," in *Mechatronics*, pp. 24–26, 2002.

[40] D. J. Lee, *Passive Decomposition and Control of Interactive Mechanical Systems under Motion Coordination Requirements*. Ph.D. Thesis, University of Minnesota, 2004.

[41] G. M. H. Leung and B. A. Francis, "Bilateral control of teleoperators with time delay through a digital communication channel," in *Proc. IEEE Allerton Conf. commun. contr. comput.*, pp. 692–701, 1992.

[42] J. E. Colgate and G. Schenkel, "Passivity of a class of sampled-data systems: application to haptic interfaces," in *Proc. American Control Conference*, pp. 3236–3240, 1994.

[43] S. Stramigioli, C. Secchi, A. J. van der Schaft, and C. Fantuzzi, "A novel theory for sampled data system passivity," in *Proc. IEEE/RSJ Int. Conf. Intelligent Robots and Systems*, pp. 1936–1941, 2002.

[44] C. Secchi, S. Stramigioli, and C. Fantuzzi, "Digital passive geometric telemanipulation," in *Proc. IEEE Int. Conf. Robot. Auto.*, pp. 3290–3295, 2003.

[45] C. Secchi, S. Stramigioli, and C. Fantuzzi, "Dealing with unreliabilities in digital passive geometric telemanipulation," in *Proc. IEEE/RSJ Int. Conf. Intelligent Robots and Systems*, pp. 2823–2828, 2003.

[46] P. Berestesky, N. Chopra, and M. W. Spong, "Discrete time passivity in bilateral teleoperation over the internet," in *Proc. IEEE Int. Conf. Robot. Auto.*, pp. 4557–4564, 2004.

[47] P. Berestesky, N. Chopra, and M. W. Spong, "Theory and experiments in bilateral teleoperation over the internet," in *Proc. IEEE Int. Conf. Control Aplications*, pp. 456–463, 2004.

[48] S. Lee and H. Lee, "Modeling, design, and evaluation of advanced teleoperator control systems with short time delay," *IEEE Trans. Robot. Automat.*, vol. 9, no. 5, pp. 607–623, 1993.

[49] T. Sheridan, "Sapce teleoperation through time delay: review and prognosis," *IEEE Trans. Robot. Automat.*, vol. 9, no. 5, pp. 592–606, 1993.

[50] G. Hirzinger, J. Heindl, and K. Landzettel, "Predictive and knowledge-based telerobotic control concepts," in *Proc. IEEE Int. Conf. Robot. Auto.*, pp. 1768–1777, 1989.

[51] T. Schlegl, M. Buss, and G. Schmidt, "Internet-based teleoperation using wave variables with prediction ," *IEEE/ASME Trans. Mechatronics*, vol. 8, no. 3, pp. 352–361, 2003.

[52] S. Sirouspour and A. Shahdi, "Bilateral teleoperation under communication time delay using an lqg optimal controller," in *IEEE Conf. Control Applications*, pp. 1263–1268, 2005.

[53] J. Nilsson, *Real-Time Control Systems with Delays*. Ph.D. Thesis, Lund Institute of Technology, 1998.

[54] N. Y. Chong, S. Kawabata, K. Ohba, T. Kotoku, K. Komoriya, K. Takase, and K. Tanie, "Multioperator teleoperation of multirobot systems with time-delay: part I-aids for collision-free control ," *Presence*, vol. 11, pp. 277–291, 2002.

[55] N. Y. Chong, S. Kawabata, K. Ohba, T. Kotoku, K. Komoriya, K. Takase, and K. Tanie, "Multioperator teleoperation of multirobot systems with time-delay: part II-testbed description ," *Presence*, vol. 11, pp. 292–303, 2002.

[56] N. Chong, T. Kotoku, K. Ohba, K. Komoriya, K. Tanie, J. Oaki, H. Hashimoto, F. Ozaki, K. Maeda, and N. Matsuhira, "A collaborative multi-site teleoperation over an ISDN," *Mechatronics*, vol. 13, pp. 957–979, 2003.

[57] X.-G. Wang, M. Moallem, and R. Patel, "An internet-based distributed multiple-telerobot system," *IEEE Trans. Syst., Man, Cybern. A*, vol. 33, no. 5, pp. 627–633, 2003.

[58] I. Elhajj, A. Goradia, N. Xi, C. M. Kit, Y.-H. Liu, and T. Fukuda, "Design and analysis of internet-based tele-coordinated multi-robot systems," *Autonomous Robots*, vol. 15, pp. 237–254, 2003.

[59] D. J. Lee and M. W. Spong, "Bilateral teleoperation of multiple cooperative robots with delayed communication: Theory," in *Proc. IEEE Int. Conf. Robot. Auto.*, 2005.

[60] D. J. Lee and M. W. Spong, "Bilateral teleoperation of multiple cooperative robots with delayed communication: Application," in *Proc. IEEE Int. Conf. Robot. Auto.*, 2005.

[61] S. Sirouspour, "Modeling and control of cooperative teleoperation systems ," *IEEE Trans. Robotics*, vol. 21, pp. 1220–1225, 2005.

[62] W.-H. Zhu, "On adaptive synchronization control of coordinated multirobots with flexible/rigid constraints ," *IEEE Trans. Robotics*, vol. 21, pp. 520–525, 2005.

[63] L. Sciavicco and B. Siciliano, *Modeling and Control of Robot Manipulators.* Springer, 2000.

[64] H. Kazerooni and M. Her, "The dynamics and control of a haptic interface device," *IEEE Trans. Robot. Automat.*, vol. 10, no. 4, pp. 453–464, 1994.

[65] G. H. Golub and C. F. V. Loan, *Matrix Computations.* The Johns Hopkins University Press, 1996.

[66] G. Strang, *Linear Algebra and Its Applications.* Brooks Cole, 2005.

[67] T. A. Johansen, "Optimizing nonlinear control allocation ," in *Proc. 43st Conf. Decision Cont.*, pp. 3435–3440, 2004.

[68] W.-H. Zhu, Y.-G. Xi, Z.-J. Zhang, Z. Bien, and J. D. Schutter, "Virtual decomposition based control for generalized high dimensional robotic systems with complicated structure ," *IEEE Tran. Robot. Automat.*, vol. 13, no. 3, pp. 411–436, 1997.

[69] W.-H. Zhu, Z. Bien, and J. D. Schutter, "Adaptive motion/force control of multiple manipulators with joint flexibility based on virtual decomposition ," *IEEE Tran. Automat. Cont.*, vol. 43, no. 1, pp. 46–60, 1998.

[70] W.-H. Zhu and J. D. Schutter, "Adaptive control of mixed rigid/flexible joint robot manipulators based on virtual decomposition," *IEEE Tran. Robot. Automat.*, vol. 15, pp. 310–317, April 1999.

[71] W.-H. Zhu and J. D. Schutter, "Experimental verifications of virtual-decomposition-based motion/force control ," *IEEE Tran. Robot. Automat.*, vol. 18, no. 3, pp. 379–386, 2002.

[72] K. Astrom and B. Wittenmark, *Computer-Controlled Systems: Theory and Design, 3rd Edition.* Prentice Hall, 1997.

[73] T. A. Johansen, *Operating Regime based Process Modeling and Identification.* Ph.D. Thesis, University of Trondheim, 1994.

[74] K. S. Narendra and J. Balakrishnan, "Adaptive Control Using Multiple Models ," *IEEE Tran. Automat. Cont.*, vol. 42, pp. 171–187, 1997.

[75] A. Rodriguez-Angeles and H. Nijmeijer, "Mutual synchronization of robots via estimated state feedback: a cooperative approach ," *IEEE Trans. Control Systems Technology*, vol. 12, pp. 542–554, 2004.

[76] Y. Bar-Shalom, X. Li, and T. Kirubarajan, *Estimation, Tracking and Navigation: Theory, Algorithms and Software.* New York: John Wiley and Sons, 2001.

[77] A. Shahdi and S. Sirouspour, "Multiple model control for teleoperation in unknown environments," in *Proc. IEEE Int. Conf. Robot. Auto.*, pp. 715–720, 2005.

[78] M. Campi, J. Hespanha, and M. Prandini, "Cautious hierarchical switching control of stochastic linear systems ," *Int. J. of Adaptive Control and Signal Processing*, vol. 18, pp. 319–333, 2004.

[79] J. Hansen and T. A. Johansen, "Transient performance, resetting and filtering in nonlinear multiple model adaptive control," *IEE Proc.*, 2006.

[80] A. V. Oppenheim, A. S. Willsky, and S. H. Nawab, *Signals and Systems*. Prentice Hall, 1996.

[81] S. Haykin and B. V. Veen, *Signals and Systems*. Wiley, 2002.

[82] K. Ogata, *Modern Control Engineering*. Prentice Hall, 2001.

[83] R. C. Dorf and R. H. Bishop, *Modern Control Systems*. Prentice Hall, 2004.

[84] P. Hacksel and S. Salcudean, "Estimation of environment forces and rigid-body velocities using observers," in *Proc. IEEE Int. Conf. Robot. Auto.*, pp. 931–936, 1994.

[85] V. B. Kolmanovskii and A. D. Myshkis, *Introduction to the Theory and Applications of Functional Differential Equations*. Kluwer Academic Publishers, 1999.

[86] V. B. Kolmanovskii and L. E. Shauikhet, *Control of Systems with Aftereffect*. Oxford University Press, 1997.

[87] K. Gu and S. Niculescu, "Survey on recent results in the stability and control of time-delay systems," *Journal of Dynamic Systems, Measurement, and Control*, vol. 125, pp. 158–165, 2003.

[88] J. Richard, "Time-delay systems:an overview of some recent advances and open problems," *Automatica*, vol. 39, pp. 1667–1694, 2003.

[89] M. Jankovic, "Extension of control lyapunov functions to time-delay systems," in *Proc. IEEE Conf. Decision and Control*, pp. 4403–4408, 2000.

[90] M. Jankovic, "Control Lyapunov-Razumikhin functions and robust stabilization of time delay systems ," *IEEE Tran. Automat. Cont.*, vol. 46, pp. 1048–1060, 2001.

[91] M. Jankovic, "Control of nonlinear systems with time-delay," in *Proc. IEEE Conf. Decision and Control*, pp. 4545–4550, 2003.

[92] G. Tao, "Model reference adaptive control of multivariable plants with delays," *Int. J. Control*, vol. 55, pp. 393–414, 1992.

[93] G. Tao, *Adaptive Control Design and Analysis*. Wiley-IEEE Press, 2003.

[94] D. D. Siljak, *Decentralized Control of Complex Systems*. Academic Press, 1991.

[95] A. G. O. Mutambara, *Decentralized Estimation and Control for Multisensor Systems*. CRC Press, 1998.

[96] E. A. Parsheva, "Adaptive decentralized delayed control of multivariable plants ," *Automation and Remote Control*, vol. 65, pp. 134–146, 2004.

[97] M. Rotkowitz and S. Lall, "Decentralized control subject to communication and propagation delays," in *Proc. IEEE Conf. Decision and Control*, 2004.

[98] B. M. Mirkin and P.-O. Gutman, "Output-feedback co-ordinated decentralized adaptive tracking: the case of MIMO subsystems with delayed interconnections," *Int. J. of Adaptive Control and Signal Processing*, vol. 19, pp. 639–660, 2005.